Effect of Ash on NH$_3$-SCR in an Integrated SCR-coated DPF for Emission Cleaning

Master thesis in the Master of Science's programme of Applied Physics (MPAPP)

ANASTASIA THEOTOKI

"Effect of Ash on NH$_3$-SCR in an Integrated SCR-coated DPF for Emission Cleaning"
Anastasia Theotoki

Department of Chemistry and Chemical Engineering

Division of Chemical Engineering
Competence Center for Catalysis

CHALMERS UNIVERSITY OF TECHNOLOGY

SE-412 96 Göteborg, Sverige
Telephone: +46 (0)31-772 1000

Collaborator: Volvo Cars

Cover:
Photograph of washcoated monolith samples with ash powder, by Anastasia Theotoki

Göteborg, Sverige 2015

"Effect of Ash on NH_3-SCR in an Integrated SCR-coated DPF for Emission Cleaning"
Anastasia Theotoki

Department of Chemistry and Chemical Engineering
Division of Chemical Engineering
Competence Center for Catalysis
Chalmers University of Technology

ABSTRACT

Nitrogen oxides (NO_x) among other pollutants have detrimental effects on both environment and human health. The selective catalytic reduction of NO_x with ammonia (NH_3-SCR) over lean-burn engines can contribute to minimizing of NO_x emissions. Cu/CHA catalysts with their chabazite framework structure, where Cu/SAPO-34 is one material, have been considered one of the most promising candidates to remove NO_x from exhaust streams, owing to their low-temperature activity and hydrothermal stability. In addition, it is crucial to remove particulate matter and this can be done in particulate filters (DPF). In order to save space and make the emission cleaning system more effective, SCR coated filters can be used.

The objective of this master thesis was to study the effect of various copper- and ash- loadings on NH_3-SCR for the application of SCR coated filters. Real ash from renovated filters was provided by Volvo Cars, and the elemental composition of the ash was examined using ICP-SFMS analysis. Both a flow reactor setup coupled with an FTIR instrument and a micro-calorimeter setup coupled with an MS instrument were utilized to investigate the catalytic activities of the samples on the NH_3-SCR reactions. The ammonia storage capacity (investigated by TPD experiments) of ash sample played an important role to understand the ash behavior.

The synthesis of zeolite catalysts and the incorporation of the concentrations of 0.05 M and 0.8 M copper into SAPO-34 zeolite catalysts using ion exchange technique were performed in this study. The XRD results confirmed the maintenance of SAPO-34 zeolite framework after ion exchange. The amounts of 2.5 and 5 g/L ash (equivalent to 17.5 and 35 mg) were then applied on the Cu-based catalysts. The ICP-SFMS analysis measured significant amounts of Fe_2O_3, CaO, P_2O_5, S, Zn, various transition metals and precious metals (Pd, Pt, Rh) in the ash sample.

Study I determined higher NO_x conversion for 0.8 M Cu/SAPO-34 compared to 0.05 M Cu-loaded sample at 150-300°C, but decreased NO_x reduction above 350°C due to NH_3 oxidation, and for both fresh samples total NH_3 conversion at high temperatures. **Study II** showed similar trends between fresh and 5 g/L ash-loaded samples, but different absolute concentrations of NO_x and NH_3. However, the ash decreased the NO_x conversion above 300°C, for both low and high Cu-loaded samples owing to NH_3 oxidation induced by the precious metals within ash. The NH_3 oxidation reaction at high temperatures was validated by DSC over ash, in agreement with the results during NH_3-SCR by flow reactor (**Micro-calorimeter study I**).

Studies III and IV revealed similar behaviour between fresh and 5 g/L ash-loaded samples, but lower NH_3 and NO_x concentrations were found at 150^oC when 2.5 g/L ash was loaded, which was unexpected. In addition, above 300^oC ash considerably reduced the NO_x conversion, likely due to high NH_3 oxidation in the presence of precious metals in ash. The suggested order of $deNO_x$ catalysts from their best to their poorest NO_x conversion activity was: fresh > Cu/SAPO-34 + 2.5g/L ash > Cu/SAPO-34 + 5g/L ash. Hence, above 300^oC the higher the ash content the poorer the catalytic activity and increased NH_3 oxidation because of precious metals in the ash.

Only 4 ppm undesirable N_2O were produced around 200^oC and about 7 ppm N_2O were formed at 550^oC for fresh 0.8 Cu-based catalyst. Increased N_2O formation (at 300-350^oC about 10-12 ppm), for samples with ash of 5 g/L compared to the fresh ones was observed, probably due to Pt residues in the ash. A CO_2 production of 12 ppm was observed above 500^oC for the 0.05 M Cu/SAPO-34 with 5 g/L ash, concluding that there might have been some coke residues in the ash that was oxidised. By contrast, formation of negligible CO_2 of just 2 ppm presented no traces of coke (consequently, no coke oxidation reaction) for the 0.8 M Cu-loaded sample with ash.

Micro-calorimeter studies II: NH_3 TPD over the ash sample revealed that after exposure to NH_3, an almost full NH_3 uptake took place, followed by an NH_3 breakthrough on the catalyst surface, and one desorption peak of *strongly bound ammonia* was observed. NO TPD showed that NO was not adsorbed on the ash, resulting in no desorption peak during the temperature ramp. Lastly, NO_2 TPD results showed that considerable amounts of NO_2 were stored in the ash sample, and therefore NO and NO_2 desorption peaks were observed during desorption period.

TABLE OF CONTENTS

1. INTRODUCTION

The following section includes the background and the scope of this master thesis, introduces the present research status and illustrates the need for current research on the topic.

1.1. Background

Nowadays, climate change and ecological footprints caused by automobile engines are issues of growing interest, since they affect human health and ecosystems. Incomplete combustion of fossil fuels as a source of energy is employed, and the automobile engines exhaust contains significant amounts of pollutants. In Europe, four main air pollutants are identified by the *National Emission Ceilings Directive (NECD)*, namely: nitrogen oxides (NO_x), sulphur dioxide (SO_2), non-methane volatile organic compounds (NMVOCs), and ammonia (NH_3) [1].

Other hazardous pollutants of exhaust gas can be particulate matter (PM), carbon monoxide (CO), hydrocarbons (HCs) and non-methane hydrocarbons (NMHCs). Soot, which is derived from the combustion of diesel fuel, is a major air pollutant and the 2nd largest cause of global warming. A minor fraction of PM produced by diesel engines is inorganic ash. It originates mainly from lubricating oil additives and, to a small extent, from trace metals in diesel fuel, engine wear and corrosion [2, 3].

According to the emissions inventory taken by the U.S. Environmental Protection Agency (EPA) in 2010, about 33% of the national NO_x emissions released into the atmosphere originates from highway vehicles [4]. Nitric oxide (NO), to a large extent, and nitrogen dioxide (NO_2) are together referred to as nitrogen oxides (NO_x). The combustion of fossil fuels is considered to be the prevailing source of outdoor NO_x emissions. The emissions are not dependent merely on the amount of nitrogen in the fuel, but also on the air-fuel mix ratio. High temperatures and oxidation-rich conditions generally favour NO_x formation in combustion. The E.U. emissions inventory report 1990–2011 under the *Long-range Trans-boundary Air Pollution (LRTAP)* convention reveals that road transport and energy production are the greatest sources of NO_x emissions in the E.U. during 2011 as shown at the chart in **Fig. 1.1.** [5, 6].
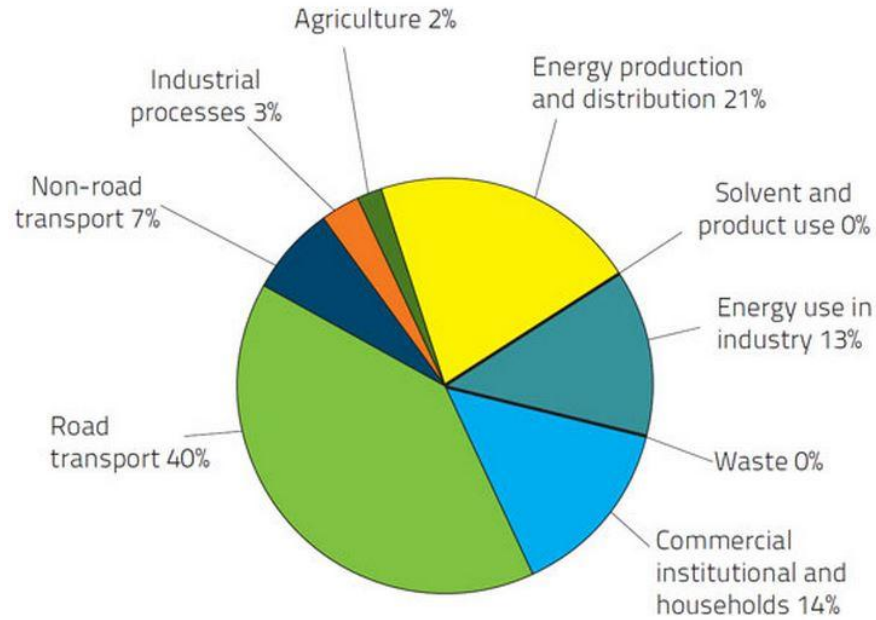
Figure 1.1: The distribution of E.U. emissions of NO_x by different sectors in 2011 [6].

1.1.1. Regulations

NO_x reduction after-treatment technologies, such as selective catalytic reduction (SCR), are required because of strict emission legislations for NO_x in mobile applications. Such stringent legislations are the US 2010, the Euro VI (to be implemented in the period 2015-2017), the LEVIII and the US Tier 3 for road vehicle engines. However, a considerable enhancement in NO_x reduction (deNO$_x$) efficiencies for diesel vehicles is necessary in order to achieve the future limitations [7, 8]. In addition to the *NECD*, the revised in 2012 Gothenburg protocol introduces new emission reduction targets for 2020 to all E.U. member states and some non-E.U. ones .

The newly proposed Non-Road Mobile Machinery regulations for 2019-20 in Europe, and the continuing developments towards real-driving emissions (RDE) standards move onwards. Besides China that started air quality initiatives, there is India's roadmap - Bharat IV in 2017, Bharat V in 2020 and Bharat VI in 2024 - on fuel quality and emissions through 2025 for clean fuels and tailpipe regulations on both NO_x and greenhouse gases (GHG) nationwide. California also investigates 80-90% heavy duty NO_x reductions for 2020, and the U.S. EPA recently proposed the next GHG standards for 2021 [8].

1.1.2. Engine Technologies

LD (light duty) and HD (heavy duty) engine technology continues showing remarkable improvements in vehicular engine efficiency. Major developments are noticed for gasoline and diesel engines to meet both the emerging NO_x and GHG regulations. Many of these developments are coming from

- combustion improvements,
- pumping loss reductions,

- waste heat recovery, and
- friction reduction.

In addition, HD engines are demonstrating over 50% brake thermal efficiency by means of new techniques that can reasonably be commercialized [8].

1.1.3. *NO_x Control*

Lean NO_x traps (LNTs) are improving in terms of sulphur tolerance and passive release of the NO_x using just temperature increases. LNTs are being combined with SCR in the LD sector to reduce urea consumption and improve system low-temperature performance. However among the lean NO_x after-treatment technologies, NO_x control is clearly focused on selective catalytic reduction (SCR), which is the dominant technology compared to alternatives. Generally, the superiority of SCR is due to

- deNO$_x$ efficiencies,
- durable performance with broad operating windows,
- reasonable cost, and
- available infrastructure.

Catalytic materials are being characterized further for sulphur degradation (poisoning) and tolerance. Low-temperature activity and performance are enhanced with high catalyst loadings, enabled by high-porosity substrates. High-temperature stability and performance are improved using higher cell-density catalysts. More information has been reported on reducing ammonia slip from SCR catalysts, as well as on understanding and improving durability of the deNO$_x$ systems [7, 8].

1.1.4. *Particulate Control*

Diesel PM (particulate matter) reduction studies are focused on the behavior of the soot cake and PM sensors. The regeneration of diesel particulate filters (DPF) using NO_2 as reducing agent, and its implications are now further quantified. The soot oxidation mainly occurs between the soot layer and the filter material, significantly decreasing the adhesion of the soot, causing it to peel off under certain circumstances. This exerts influence on the back-pressure and ash distribution, because ash particles alter the pressure drop sensitivity of the system to some degree [2].

Gasoline particulates are described to contain a wide collection of HC species, and the gasoline particulate filter (GPF) regeneration is now better understood. Ash particles can help during the soot oxidation, as well as a three-way catalyst (TWC) incorporated into the filter [8]. For mobile sources, although NO_x from gasoline is very efficiently reduced by means of TWC, this technology cannot be applied in the lean-burn gasoline and diesel engines [9].

1.1.5. *Gaseous Pollutant Control*

There are developments in gasoline gaseous emission abatement, focusing on satisfying the new U.S. regulatory standards on durability and on lean-burn gasoline emissions control.

Oxidation catalysts mainly involve solutions towards issues such as low-temperature performance with exhaust high in HC and CO, and methane oxidation. Diesel oxidation catalysts (DOC) are being optimized for the use with fuels containing higher sulphur content. It is shown that periodic rich episodes are needed to improve both DOC and methane catalyst performance by reducing oxidation poisoning. TWCs are being designed with better low-temperature oxygen storage capacity. More knowledge is reported about the effect of fuel cut-offs on catalyst deterioration. Lean-burn gasoline NO_x reduction systems using LNTs and passive SCR are showing 99% NO_x reductions and marked fuel consumption decline after using rich episodes to generate NH_3 [8].

1.2. SCRF Technology

In comparison to conventional DPF and SCR processes, the SCR coated on DPF (commonly called as SCRF) is a system which filters PM. The SCR catalyst is coated onto the walls of the DPF channels by washcoating, and hence, the SCR and DPF functionalities are integrated into one. As illustrated in **Fig. 1.2.**, phenomena such as the PM filtration from a DPF, the passive soot oxidation in a soot cake and the SCR reactions in the substrate wall occur within the SCRF unit [10, 11].
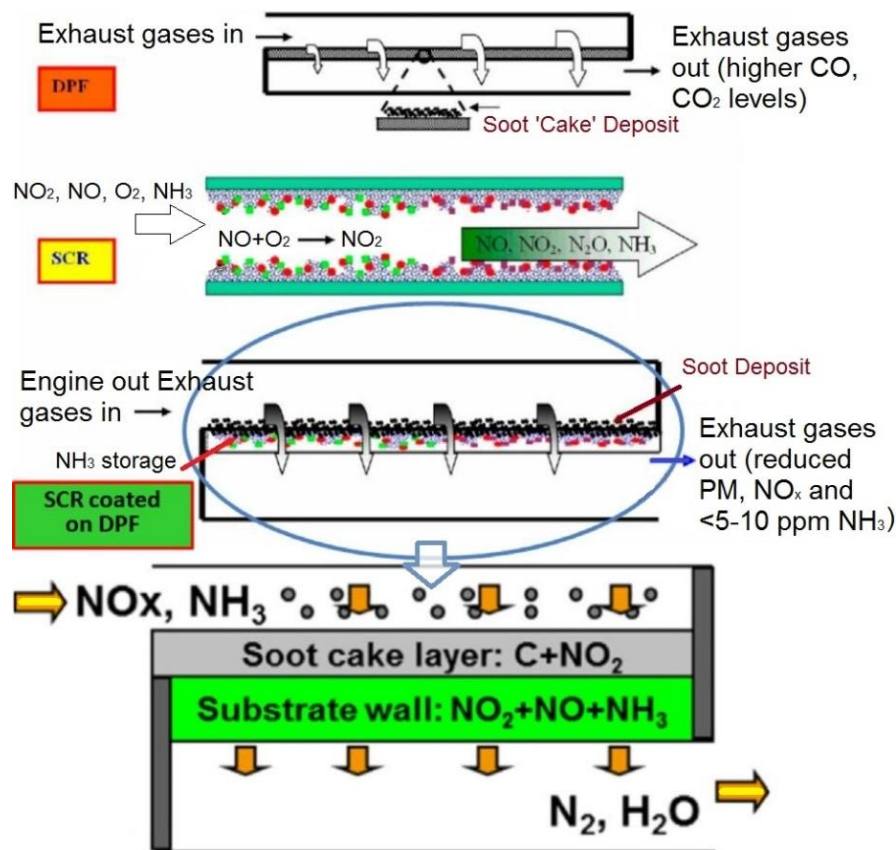

Figure 1.2: Schematic of physical and chemical processes in a wall-flow substrate channel for SCRF (Adapted from [7, 10, 11]).

The SCR catalysts used in SCRF are similar to those deployed in the conventional SCR, apart from that the washcoat has to be optimised in the filter to decrease the pressure drop Δp, and increase the conversion efficiency. One of the reasons of developing an SCRF system is to achieve a good NO_x conversion, especially in cold start cycles. An 86% NO_x conversion has been reported during cold start and over 90% $deNO_x$ efficiency under steady-state conditions has been achieved for Cu-based zeolite SCRF catalysts. The advantages of the SCRF system are summarized as

- packaging benefits, and
- better light-off behaviour of SCRF catalyst.

Particularly, packaging space and weight are decreased and thus overall cost of the exhaust system is reduced. Furthermore, it allows for faster light-off of $deNO_x$ function because the SCRF is now mounted in a more favourable position in relation to the engine, with superior DPF regeneration efficiency and low thermal losses. Therefore, an SCRF entails a combined cost-efficient and conversion-efficient novel technology that reduces NO_x and soot simultaneously. The SCRF exhibits lower peak substrate temperatures (~750°C) than the conventional DPF due to the ability of the zeolites to catalyse soot oxidation so that, in case of uncontrolled soot regeneration, substrates can be preserved [11, 12]. There are some challenges, though, that need to be addressed concerning the

- applicability of merely zeolite-based SCR catalysts,
- high temperatures during DPF regeneration, and
- NH_3 storage dependence on soot load.

In fact, high thermal durability and robustness of the SCR catalysts coated on DPF are obligatory. Moreover, high SCRF $deNO_x$ performance is required in the 200-350°C temperature range for vehicles. During active DPF regenerations (450-700°C), high stress of SCR coating and uncontrolled NO_x emissions need to be managed as well [7, 10-12].

A major drawback is that the wall-flow substrate limits SCRF catalyst content due to the pressure drop restriction, while high SCR loading necessitates high $deNO_x$ efficiency. For this reason, the filter porosity plays a significant role in the SCRF system contrary to the traditional DPF. The SCR washcoat needs to be homogeneously coated inside the DPF pores, rather than on the substrate surfaces, allowing space for gas flow and soot storage. The back-pressure along SCRF catalysts can be minimized, by using high-porosity filters and an optimal washcoating [7, 13].

1.3. Composition and Behaviour of Soot and Ash

1.3.1. *Ash and Soot Composition*

Fly ash from Waste-to-Energy (WtE) contains alkali (mainly Ca, Na and K), anions (mainly Cl and sulfate), toxic heavy metals (mainly Zn) and organic pollutants. Due to the high amount of toxic and corrosive components, fly ash is considered as hazardous waste. Removal of both soot and ash PM from the exhaust gas of diesel engines is an ongoing aim, largely

accomplished by using different exhaust after-treatment methods. To achieve this, the utilization of DPFs with a filtration efficiency of 95-99% is considerably helpful. Soot PM enclosed in the DPF is oxidised and removed *partly* continuously during passive regeneration (upstream of DPF at 200-400°C) and *partly* gradually during active regeneration (upstream of the DPF at 550-650 °C) [14].

**Figure 1.3-1: Fly ash powder, as a mineral product from industrial coal combustion.**

Diesel soot particles are a few tens of nanometers in diameter, while diesel ash PM range from tens of nanometers down to a few nanometers in size [15]. Investigation of soot and ash PM deposited in DPFs operating with biofuel or diesel show for ash that mainly Ca-S- and P-containing compounds range in size between 50 and 300 nm. Smaller ash particles are less common and can favour the formation of aggregates. The existence of Fe-Cr-Ni fragments within the ash is ascribed to engine wear, since the fragments probably come from abraded engine parts. Pt particles (50-400 nm) suggest that the DOC upstream of the DPF experiences aging effects, which is confirmed by visible radial cracks on the DOC coating [16].

1.3.2. Ash and Soot Behaviour

In contrast to soot, the ash particles stay inside the DPF, are deposited on the DPF surface and accumulate into the channel walls of the filter. Ash accumulation and behavior in the DPF is of utmost importance, as it reduces the filter's effective volume and its operational lifetime, thus impacting the engine performance [8, 16]. More ash PM generated from biofuel engine cannot be chemically withdrawn and slowly overloads the DPF at the expense of engine efficiency [17, 18].

The amount of soot accumulated in the filter prior to regeneration significantly affects the level of ash migration from the channel walls to the back of the filter. Particularly, a thicker soot cake demonstrates less adhesion due to proportionately more gaps between soot and filter, as well as it causes higher drag forces from the gas acting on the soot. Large (500-800 µm) parts of the soot cake, containing ash particles, detach from the filter surface and migrate to the filter channels. By contrast, when a small amount of soot accumulates in the filter (cf. when a thicker soot cake is on) prior to regeneration, it is expected that more ash will be deposited on the channel walls [19].

The collapse of the soot layer, as illustrated in the scanning electron microscope (SEM) images in **Fig. 1.3-2.**, affects the middle-to-outlet zone of the filter. At first, gaps are formed between the soot and the wall due to soot oxidation in the proximity of the catalyst (soot in un-catalysed filters does not separate from the wall). But under certain conditions, the unstable soot layer becomes concave, separates from the DPF walls, collapses into the channel, causing a sudden restriction and an increase in pressure drop Δp, and ultimately clogs the DPF. Such conditions include high load, extended highway driving, soak period, excessive humidity and passive DPF regeneration [20].
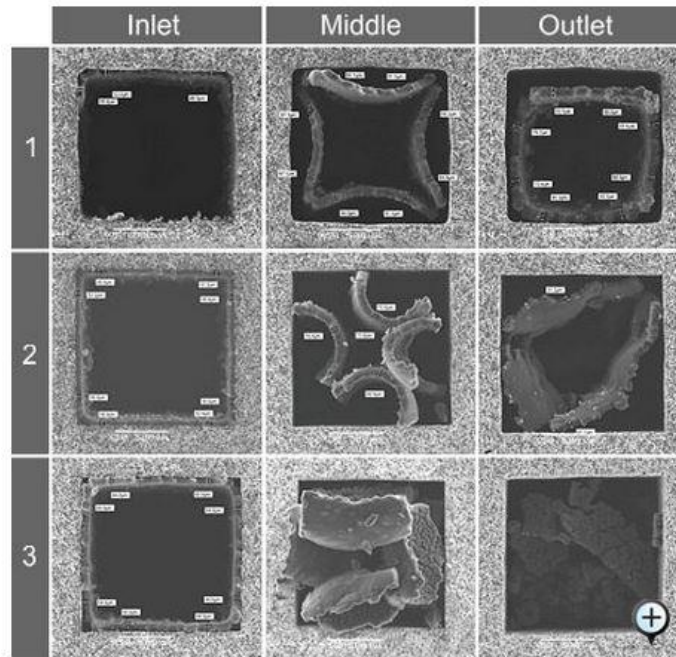
Figure 1.3-2: SEM analysis of soot plugging in DPF samples. 1: Formation of concaved soot layer; 2: Soot layer collapse; 3: Channel plugging [20].

After long periods of soot build-up followed by cooling (e.g. overnight), Δp increases suddenly across the filter during driving, but not during an idling period. Upon cooling, water condenses within the soot layer. The rapid heating can cause the wet soot to expand and break off, increasing the back-pressure of the filter. Idling after soak period allows the water to slowly retire, alleviating the magnitude of the problem [21].

When an SCR catalyst is incorporated into the DPF, the passive regeneration behavior is compromised due to the loss of NO_2. However, recent studies show that a quantified engine management, over both temperature and NO_x/soot ratios, as well as catalyst formulations enable a shift from the non-passive to the passive regeneration mode [22].

The three-way catalyst (TWC) is found to be an important component that reduces PM emissions (e.g. volatile organics and soot). Ash plays a more fundamental role in the oxidation reactivity of gasoline-direct-injection (GDI) soot than that of diesel soot, because GDI soot contains a higher proportion of ash than diesel soot. Crystalline structures of GDI soot are

slightly less ordered than those of diesel soot, except for the idling period, and are not altered dramatically under engine operating conditions. Soot chemistry (hydrocarbons, weakly bonded carbon, ash) is a major factor for the enhanced oxidation of GDI soot [23].

1.4. Thesis Objective

The objective of this work is to examine the combined effects of ash and metal loading (Cu, in this research) on the NH_3-SCR reactions. Different concentrations of Cu and ash are to be used in order to investigate their influence on the SCR process. Real ash from renovated filters is provided by Volvo Cars and used in this master thesis. The chemical composition of the ash is examined using *Inductively Coupled Plasma-Sector Field Mass Spectrometry* (ICP-SFMS) analysis. Moreover, the effect of ash is predominantly examined in a flow reactor, where catalysts coated with ash are placed in quartz tubes and exposed to different gases using mass flow controllers (MFCs). The outlet gases are monitored using an FTIR analyser. Further micro-calorimetric studies are to be performed over the ash sample for its chemical properties and influence on the NH_3-SCR reactions.

2. THEORY

The following section is a brief and comprehensive description of the SCR chemistry, the catalysts structure and function on NH_3-SCR activity, and the wet ion exchange (WIE) method.

2.1. Urea- or NH_3- SCR Chemistry

The need for NO_x reduction through urea-SCR catalysts arises given the proven performance of urea-SCR in mobile applications. Many attempts are still made to develop superior-efficiency catalysts with wide temperature windows, noteworthy durability and NH_3 storage capacity, as well as to optimize combinatory after-treatment systems (ATS) to meet the NO_x emission regulations [24].

Urea NH_2-CO-NH_2, as selective reducing agent or reductant, is preferred for mobile applications due to safety and negligible toxicity issues concerning storage and transportation of NH_3. It is an ammonia carrier or storage compound for ammonia. If urea, as an aqueous solution, is injected into hot exhaust gas, it decomposes in three steps, physically separated in time and space.

    i.   Evaporation of water: ***NH_2-CO-NH_2 (aqueous) → NH_2-CO-NH_2 (molten) + H_2O (gas)*** *(1)*
    ii.   Thermal decomposition of urea: ***NH_2-CO-NH_2 (molten) → NH_3 (gas) + HNCO (gas)*** *(2)*
    iii.   Hydrolysis of isocyanic acid: ***HNCO (gas) + H_2O (gas) → NH_3 (gas) + CO_2 (gas)*** *(3)*

The initial step is equivalent to melting of urea and no catalyst is involved. The second step occurs along the exhaust pipe prior to catalyst, and involves molten urea heating up and hence decomposing. The final step happens on the catalyst surface and NH_3 arises as a product.

The overall urea decomposition is shown in the reaction:
***NH_2-CO-NH_2 + H_2O → $2NH_3$ + CO_2*** *(4)*
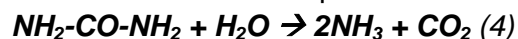
in which 1 mol of urea generates 2 mol of NH_3. The stoichiometric molar ratio in typical SCR reactions is NH_3:NO_x = 1:1 and therefore the stoichiometric balance can be NH_2-CO-NH_2:NO_x = 1:2 [25]. Nitrogen oxides (NO_x) in diesel exhaust are composed by a large fraction of ~95% NO and 5% NO_2.

Therefore, the main reaction of SCR with NH_3 basically is the *"standard SCR"*:
$4NH_3$ + 4NO + O_2 → $4N_2$ + $6H_2O$ *(5)*
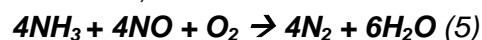
for stoichiometry NH_3:NO=1:1 and consumption of some oxygen. The reaction:
$4NH_3$ + 6NO → $5N_2$ + $6H_2O$ *(6)*
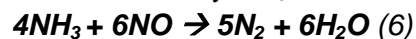
in the absence of O_2 consumption, changes the stoichiometry of NH_3:NO to 2:3, is much slower and is therefore no relevant to or can be neglected in lean combustion gases. The reaction rate of *"fast SCR"* reaction:
$4NH_3$ + 2NO + $2NO_2$ → $4N_2$ + $6H_2O$ *or* ***$2NH_3$ + NO + NO_2 → $2N_2$ + $3H_2O$*** *(7)*
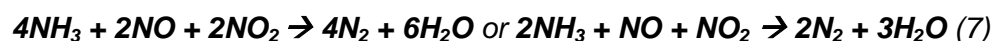
with equimolar amounts of NO_2 and NO (1:1 mixture), is much higher than that of *"standard SCR"* reaction (5). An increased NO_2 fraction, which enhances the SCR activity, can be obtained by placing a properly sized DOC upstream of the SCR system.

If NO_2/NO exceeds 50%, the overall SCR reaction*:*
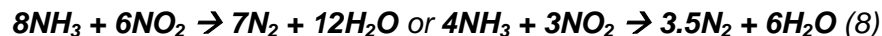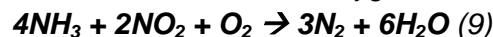**$8NH_3 + 6NO_2 \rightarrow 7N_2 + 12H_2O$ or $4NH_3 + 3NO_2 \rightarrow 3.5N_2 + 6H_2O$ (8)**

with pure NO_2 and without oxygen is again slower than reactions (5) and (7). Both of them result in a 1:1 consumption of NO_x and NH_3 however the stoichiometry of the reduction of NO_2 is not clear. The reaction with oxygen:
$4NH_3 + 2NO_2 + O_2 \rightarrow 3N_2 + 6H_2O$ (9)

may instead lead to another stoichiometry [7, 26].

Regarding the side reactions that compete with the desired reactions, the common catalysts form nitrous oxide (N_2O) at both low and high temperatures. These side reactions can either produce secondary emissions or consume ammonia unproductively. One of the possible reactions leading to N_2O is:
$4NH_3 + 4NO + 3O_2 \rightarrow 4N_2O + 6H_2O$ (10)
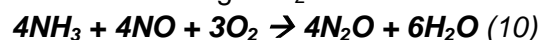
- At higher temperatures, undesirable oxidising properties of SCR catalysts arise, such that ammonia may be consumed by oxygen and possibly form additional NO or N_2O. The reaction: **$4NH_3 + 3O_2 \rightarrow 2N_2 + 6H_2O$ (11)** represents the oxidation of NH_3 to N_2, thus limiting the maximum NO_x conversion.
- At lower temperatures <200°C ammonium nitrate NH_4NO_3 can be formed, according to the reaction: **$2NH_3 + 2NO_2 \rightarrow NH_4NO_3 + N_2 + H_2O$ (12)** in the NO_x feed, and contains NO_2. This ammonium nitrate may decompose and contribute to the formation of N_2O [27, 28].

In general, one of the problems with NH_3-SCR is that, depending on the conditions, the formation of N_2O or explosive NH_4NO_3 has been observed, which affects both emission quality and block catalyst pores leading to deactivation [27]. The formation of the latter can be avoided by maintaining the temperature of the system above 200°C, although this is not favourable for wide-scale applications [26]. This elevated temperature margin is also required to obtain a complete decomposition of urea to NH_3 [1].

2.2. NH₃-SCR Catalysts

2.2.1. *V-based SCR Catalysts*

Vanadia-based SCR catalysts are vanadium pentoxide (V_2O_5) catalysts first commercialized for NO_x emission reduction from both stationary and mobile sources. V_2O_5 is the active species in the SCR process, anatase titania (TiO_2) constitutes the support of the catalyst, while tungsta (WO_3) works as a physical and chemical promoter inhibiting a certain function of anatase phase of titania. Because of their cost and performance advantages, V-SCR catalysts are considered good catalysts in terms of deNO$_x$ efficiency and thermal stability, but improvements are needed.

The commercial V-SCR catalyst has demonstrated benefits of high activity for NO_x reduction at intermediate temperature range (300-450°C), and of resistance to sulphur, hydrocarbon and lubricant poisoning. A newly developed V-SCR catalyst presented higher temperature tolerance, up to 650°C. Nevertheless, for mobile applications where both DPF and SCR catalyst are required, active DPF regeneration can severely deactivate the V-SCR catalyst. This phenomenon decreases the catalyst surface area and results in lower activity. In addition, the release of volatile vanadium compounds, such as V_2O_5, from these catalysts at high temperatures (>650°C) is a concern because of its toxic nature [1, 26, 28, 29].

2.2.2. *Zeolite SCR Catalysts*

Zeolites are (hydrated) crystalline aluminosilicates with a well-defined microporous structure, interestingly referred to as "molecular sieves" because of their open-pore matrix structure. Due to their ability to sort out an atom or molecule based on its size and shape (dimensions), thus controlled by the framework, zeolites let small molecules pass through but trap larger ones. Since the pores in a synthetic zeolite have a fixed size and shape, zeolite catalysts can work selectively on certain molecules, mainly as shape-selective catalysts. This is how water molecules and alkali or alkaline-Earth metal cations become part of a zeolite crystal and chemical reactions readily take place. Zeolites can also adsorb and desorb liquids, especially gain and lose water molecules very easily (*reversible dehydration*) [1, 30].

Whenever both DPF and $deNO_x$ catalysts are needed, zeolites are the preferred catalysts for automotive applications due to their

- low price,
- nontoxicity,
- high SCR activity and selectivity to N_2,
- impressive performance at low temperatures,
- superior thermal durability at high temperatures, and
- outstanding efficiency at high space velocities.

Zeolite types with porous networks, such as zeolite beta (BEA), chabazite (CHA), faujasite (FAU), ferrierite (FER), modernite (MOR) and modernite framework inverted (MFI) have proven to be exceptionally active $deNO_x$ catalysts for NH_3-SCR applications. In particular, transition metal - copper (Cu) and iron (Fe) - exchanged MFI zeolite systems (Cu/ZSM-5 and Fe/ZSM-5) have received much attention as promising catalysts for reduction of NO_x emissions [1, 9, 26, 31-33].

2.2.3. *Zeolite Structure*

The zeolite structure consists of tetrahedra of four O anions that surround a Si or Al ion, resulting in tetrahedra of alumina (AlO_4) and silica (SiO_4). The tetrahedra are interlinked so that each O anion is shared by another silica or alumina tetrahedron, and are arranged so that no aluminum may share O with a second aluminum. Both MFI (ZSM-5) and BEA can be synthesized in a wide range of SiO_2/Al_2O_3 ratios. The number of aluminum ions or the $M_{(exchanged)}/Al$ ratio in the zeolite determines the amount of transition metal ions that can be

exchanged into the zeolite. Due to the fact that Al has one unit charge lower than Si, the negative charges are balanced by framework cations, such as protons or other positive ions. Hence, the so-called Brønsted acid sites in zeolites can be ion-exchanged with metal ions, in that zeolites can exchange other positively charged ions for the metal ions originally trapped inside them, by various preparation methods [1, 26, 34].

Regarding framework, for example, zeolites with BEA, MFI and CHA structure have large, medium and small average pore diameters respectively. According to the *Database of Zeolite Structures*, the BEA and MFI framework structures can contain 12 and 10 O-atoms in the window opening respectively, whereas small-pore zeolites with CHA structure (**Fig. 2.2-1.**) have a smaller window size with 8 O-atoms on their framework topology [35, 36].
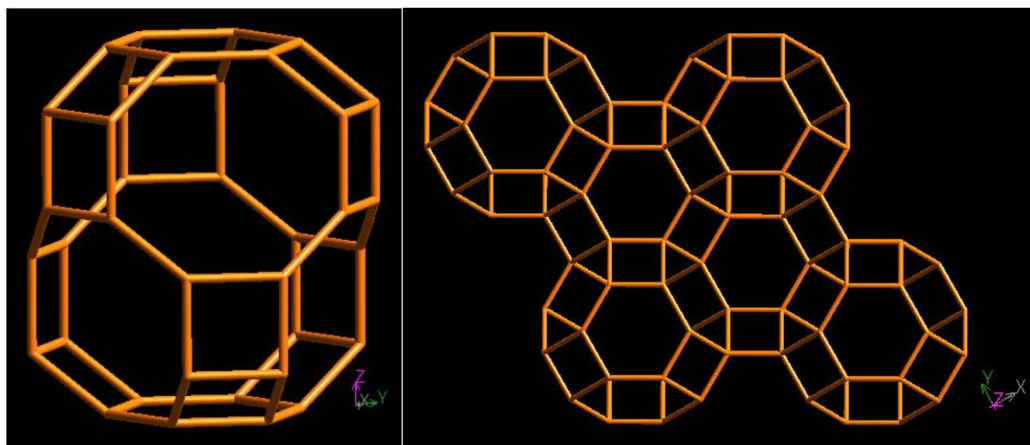
Figure 2.2-1: Cage and channels viewed normal to [001] (left) and along [001] (right) of the CHA framework type (*Database of Zeolite Structures*) [35].

2.2.4. SAPO-34 Structure

Isomorphously substituted aluminophosphates or rather silico-aluminophosphates (SAPO), are a relatively new family of "molecular sieves" with a porous CHA structure and acidity similar to other zeolite types, but with a much higher thermal stability. The crystal structure of SAPO-34 is reported to remain stable up to 1000°C even in the presence of humidity, and SAPO-34 containing Cu or Fe seems to exhibit superior thermal stability [26].

Comparing acidity, at low temperatures, there are adsorbed NH_3 molecules on weak Brønsted acid sites (surface hydroxyl as T-OH, where T=Si, P, Al) and Lewis acid sites due to Cu species. On the contrary, at high temperatures, adsorbed NH_3 molecules appear both on strong Brønsted acid sites (Si-OH-Al) and newly created Lewis acid sites by Cu^{2+} species [37, 38]. Without any hydrothermal treatment, it is shown that the ion-exchanged Cu/SAPO-34 exhibits higher NH_3-SCR activity than the *precipitated* sample, suggesting that the isolated Cu ions at the exchange sites most probably are the active sites [38].

The CHA structure of SAPO-34 (typical cubic crystal), nevertheless, is unchanged after hydrothermal aging of ion-exchanged samples. A reason for this phenomenon is that CuO clusters initially *precipitate* on the SAPO/34 external surface and then migrate from the external

surface to ion-exchanged sites inside the pores of SAPO-34 zeolite. They get incorporated and dispersed as isolated Cu ions in Cu/SAPO-34 microporous framework during the treatment. Particularly, this means that they are transported into the micro-cavities of SAPO-34 and form isolated Cu ions at the exchange sites, which are the most stable locations for Cu ions in the SAPO-34 framework. This is a direct confirmation that the prevailing active sites for NH_3-SCR reactions are occupied by isolated Cu ions, which are the most stable sites of SAPO-34 [39].
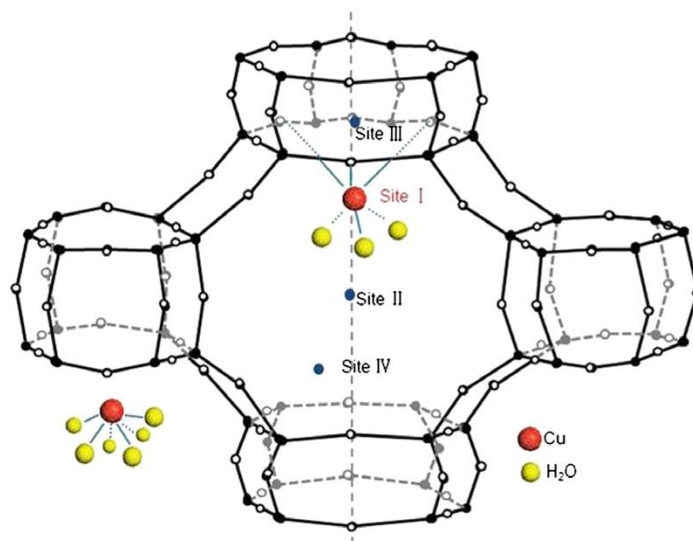

Figure 2.2-2: Diagram of the unit cell of SAPO-34. Each black sphere stands for Al, P or Si and each white sphere for O [40].

In general, four Cu species exist within Cu/SAPO-34 and these species are CuO clusters on external surface, isolated Cu^{2+} ions, nanosized CuO and Cu^+ ions [39, 40]. Studies show that isolated Cu^{2+} sites are coordinated to three oxygen atoms and three H_2O molecules. These ions are dislocated from the six-ring window into the ellipsoidal cavity of SAPO-34 at *Site I* (**Fig. 2.2-2.**). In particular, isolated Cu^{2+} ions moving towards this cavity indicate that this site is the most accessible site to the adsorbates, such as molecular NO [40].

2.2.5. *Hydrothermal Stability*

The main drawback of zeolite SCR catalysts is their lack of hydrothermal stability. At high temperatures and in the presence of water vapour, the zeolite framework is compromised; combined effects of *dealumination* and undesired ion migration into the framework diminish the SCR capability. However, recent reports have shown that the Cu-exchanged CHA zeolite systems (e.g. Cu/SSZ-13 and Cu/SAPO-34) are hydrothermally stable and among the leading candidates for ammonia SCR applications so far. As shown in **Fig. 2.2-3.**, before hydrothermal treatment the Cu/ZSM-5 crystals are fairly smooth and uniformly shaped, while Cu/ZSM-5 loses its crystallinity after treatment. By contrast, Cu/SSZ-13 maintains the same hexagonal morphology and surface texture before and after hydrothermal treatment [1, 31, 32, 41-44].
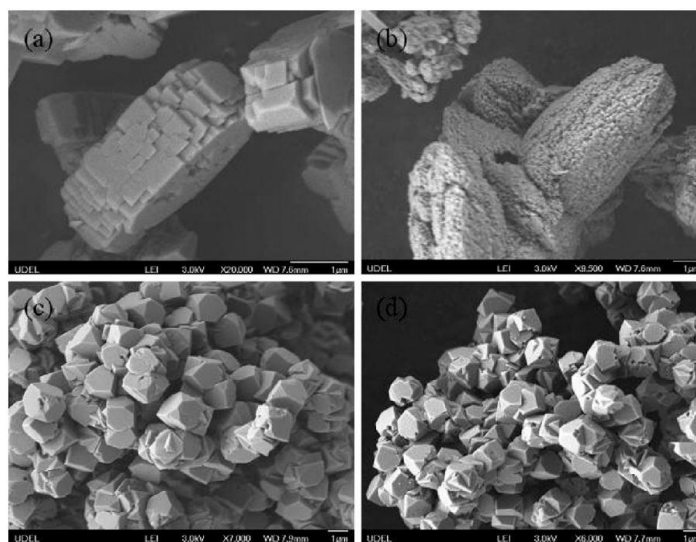
Figure 2.2-3: SEM images of Cu/ZSM-5 (a, b) and Cu/SSZ-13 (c, d) before and after hydrothermal treatment [32].

The NO_x reduction capabilities of Cu/ZSM-5, Cu/SSZ-13, -16 and Cu/SAPO-34 are shown in **Fig. 2.2-4.**, after hydrothermal treatment of 14h. It is apparent that after treatment the $deNO_x$ performance of Cu/ZSM-5 is diminished at low temperatures, while Cu/SSZ-13, -16 and Cu/SAPO-34 still demonstrate good $deNO_x$ capabilities. That decrease in the activity is because of *dealumination* of the MFI framework. In particular, during hydrothermal treatment, aluminum hydroxide compounds such as $Al(OH)_3$ exit the MFI framework causing structural defects which result in the lower $deNO_x$ capability. On the contrary, $Al(OH)_3$ cannot exit the small-pore windows of CHA framework leading to similar $deNO_x$ capability before and after hydrothermal treatment. Hence, metal exchanged CHA type zeolites (SSZ-13, -16 and SAPO-34) are indeed promising catalysts for NH_3 based SCR applications and expected to meet the future needs [31, 32, 41, 43].
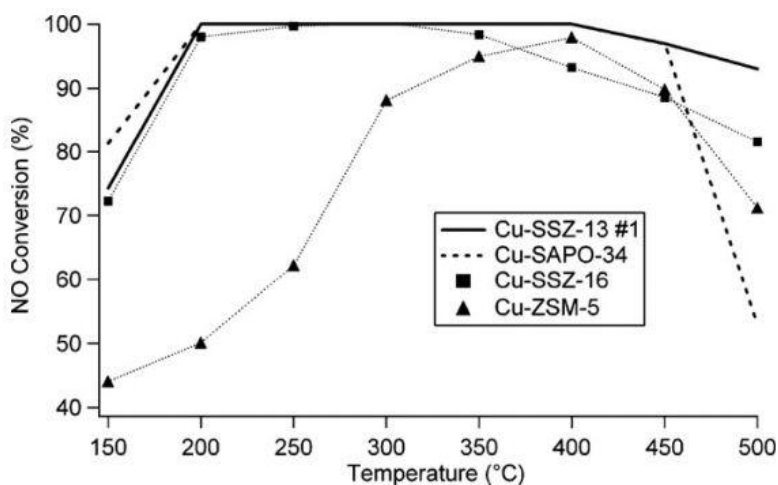
Figure 2.2.-4: NH_3-SCR activity of Cu/SSZ-13, Cu/SSZ-16, Cu/SAPO-34 and Cu/ZSM-5 after 14h hydrothermal treatment [32].

2.3. Catalyst Synthesis by Ion Exchange Methods

Metal-exchanged zeolites, especially Cu- and Fe- promoted zeolite catalysts, are most widely studied and commonly used for NH_3-SCR owing to their availability, high activity and selectivity, and good redox capacity useful for NO_x reduction.

Cu-based zeolites are usually more active in the low-temperature range (<300°C) while Fe-based zeolites are more active at higher temperatures (>300°C) during steady-state conditions when *"standard SCR"* reaction (5) is predominant. However, for mobile applications where a DOC is placed upstream of the SCR catalyst, *"fast SCR"* reaction (7) dominates and Fe-based zeolites have shown higher activity than Cu-based zeolites [45]. In addition, Fe ion-exchanged zeolites have exhibited relatively higher resistance to sulphur poisoning as compared to Cu ion-exchanged zeolites [46, 47]. However, for the Cu-exchanged CHA zeolites the high activity at low temperatures is a large advantage.

There are quite a few different methods used for the introduction of active Cu or Fe species into zeolites. One of the most common methods, the wet ion exchange (WIE), enables one to exchange Cu^{2+}, Fe^{2+} or Fe^{3+} ions in aqueous solutions. An alternative method is to introduce the metal ions into the zeolite by solid-state ion exchange (SSIE) in the absence of solution. SSIE requires a high-temperature regime, which restricts the method applicability to just thermally stable zeolites.

Other methods can include the sublimation or chemical vapour deposition (CVD), ex-framework isomorphous substitution, "mechanochemical" route (MR), improved wet ion exchange (IWIE) and incipient wetness impregnation [26, 48, 49].

### 2.3.1. *Wet Ion Exchange (WIE)*

Aqueous or liquid or wet ion exchange (WIE) is the most preferred, among others, technique for preparing ion-exchanged zeolite catalysts. The zeolite in the H- and NH_4- form is added to a metal salt solution under continuous agitation in an inert atmosphere or air. After the exchange process, the slurry is filtered and washed with deionised (DI) MilliQ water [48].

The optimal pH conditions are also considered an important factor in producing highly active NH_3-SCR catalysts. Multivalent ions, such as Cu^{2+}, Fe^{2+} or Fe^{3+}, cannot be exchanged as efficiently as monovalent ones due to the positive charges. These charges have to be balanced by individual negative charges in the zeolite framework. This issue necessitates control over the pH to favour the formation of monovalent oxy-, hydroxy- or oxygen- bridged ions.

As a result of metal-ion exchange, isolated Cu^{2+}, Fe^{2+} or Fe^{3+} ions, metal oxide clusters or aggregates, as well as bridging oxygen in binuclear species may be formed. Nevertheless, a precise control of the pH inside the zeolite pores is hard to achieve. The local pH within the pores is anticipated to be rather high, such that even *precipitation* of metal hydroxides (with a subsequent formation of metal complexes) is a concern. This is because the remaining protons shift the equilibrium between the isolated ions and the corresponding oxo- or hydroxo- ions in favour of the former [26, 48, 50, 51].

Another disadvantage of WIE method with transition metals, such as Cu, Fe or Ag, is that it is improbable to exploit the full exchange capacity of the narrow pores. This means that the percentage of the catalyst sites that can be occupied by the metal ions may be limited to less than 50% in WIE. The existence of stable metal complexes in solution is a requirement on preparing ion-exchanged zeolites in aqueous media with a $M_{(exchanged)}/Al$ ratio of 1.

Whenever H_2O is present during or after the exchange, hydrolysis takes place and so this ratio cannot be obtained, which prevents exchange levels from increasing above 50%. This hydrolysis of the metal aquo-complexes to metal oxy-hydroxides competes with the exchange process. It is also proven that the formation of different Brønsted acid sites (hydroxyl groups) occurs both during the exchange process and upon drying of the zeolite. It is pointed out that over-exchanged (Fe/Al=1) zeolites cannot be prepared easily by traditional WIE. Over-exchange is one of WIE preparation goals, but it is not vital for gaining high catalytic activity [48, 52].
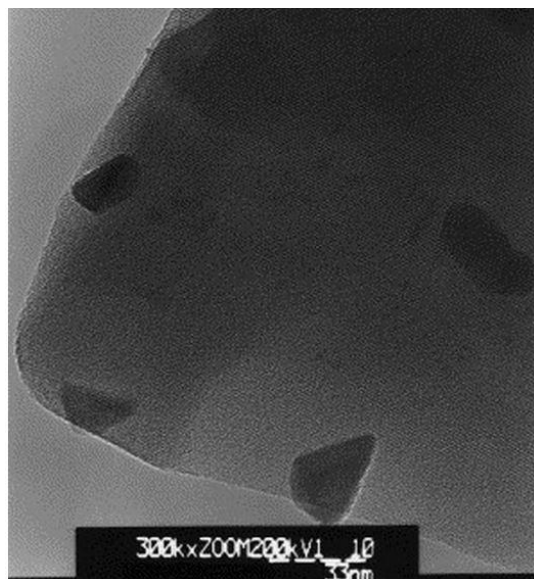
Figure 2.3-1: High-resolution electron micrograph (HREM) of zeolite UOP after calcination [50].

Metal oxide aggregates in the zeolite are observed to appear in a way that does not depend on the exchange metal or method, but instead on the metal concentration [53]. The appearance of aggregates of different sizes (oligonuclear clusters or particles) thus increases with ion exchange degree and diffusion time, but it may be prevented by applying *alkaline leaching* to de-agglomerate the zeolite crystals. However, it cannot be completely avoided since even minor amounts of O_2 in aqueous solutions help in oxidation [26, 30, 51, 54, 55].

The gelatinous hydroxides partially block the zeolite pores and lead to the formation of inactive metal oxides on the external zeolite surfaces [51]. Most of the *precipitate*, blocking the pores and preventing the exchange, is removed upon extensive washing, whereas the remaining species are transformed into metal oxides (dark particles in **Fig. 2.3-1.**) during subsequent thermal treatment and calcinations.

This phenomenon results in fairly higher activity, due to the elimination of water remaining in the zeolite pores from the "washing" step, prior to the formation of the undesired inactive clusters. Aggregated species are formed at the expense of mononuclear sites, upon calcination at high temperatures, and aggregates formation is slightly favoured by calcination with higher heating rates and by large Si/Al ratios of the catalyst [49, 50, 52].

2.3.2. WIE for SAPO-34 Synthesis

A drawback related to using aqueous solutions is that the exchange process has to be repeated several times to acquire a high ion exchange level, especially when small-pore zeolites are tested. For such zeolites, it has been reported that exchanges might be more effectively performed at temperatures of ~80°C to decrease the hydration sphere in size and enhance the metal ion diffusion. For SAPO-34, the presence of small-pore windows in combination with the hydrophilic nature of silico-aluminophosphates makes the introduction of catalytically active Cu species more difficult during WIE [26, 32, 36, 43, 48].

In order to secure the SAPO-34 support from the adverse presence of moisture (H_2O) at low temperatures and improve its stability, a Cu^{2+} protection mechanism is suggested. With increasing Cu content, the Brønsted OH group decreases, such that protons in SAPO-34 framework are replaced by Cu^{2+} species that stabilize broken Si-O-Al bonds [56, 57].

2.3.3. Influence of Metal Content and Si/Al Ratio on Brønsted Acid Sites

The type and loading of the metal inside the ion-exchanged zeolite affects not only the NO_x reduction and the NH_3 oxidation, but also the Brønsted acidity, which is important for NH_3-SCR over ion-exchanged zeolites. Moreover, the total framework acidity (i.e. the number of acid sites) and thereby the capacity to introduce metal ions at exchangeable sites is determined by the Si/Al ratio and vice versa. This is because the Brønsted acid sites of the zeolite are created by the Al nuclei or centers. Typically, high Al contents or low Si/Al ratios are favourable for high NO conversions and SCR activities [58, 59].

More metal ions after substitution of NH_4^+ (or H^+) usually result in a drop of the number of Brønsted acid sites [60]. Having low metal content, more acid sites are available for NH_3 adsorption and the metal ions are evenly distributed. If the metal content is high, fewer acid sites are free and this is favourable for undesired metal oxide particles and clusters out of the zeolite framework, which are responsible for NH_3 oxidation [58].

However, too high ion exchange degree does not influence the NH_3-SCR activity, due to the fact that Brønsted acidity is too much decreased. As long as adequate Brønsted acid sites exist, the level of metal exchange appears to be limited to some extent [26]. The H-forms of zeolites are active, however the activity of the proton sites is significantly lower when compared to the copper sites [61].

Furthermore, the Brønsted acidity in turn exerts influence on the SCR activity of the metal ion sites (e.g. Fe^{3+} ions). In the course of SCR process, gaseous NH_3 molecules are hastily adsorbed on the Brønsted acid sites to form NH_4^+ ions, and NO molecules are oxidised to NO_2 by oxygen on metal ion sites [60]. NO_x reduction most likely occurs on the Brønsted acid sites,

and the metal ions oxidise NO to NO_2. Therefore, the SCR activity requires two site types: the Brønsted acid sites for NH_3 adsorption, and the metal ion sites for NO oxidation to NO_2 (*dual mechanism*) [26].
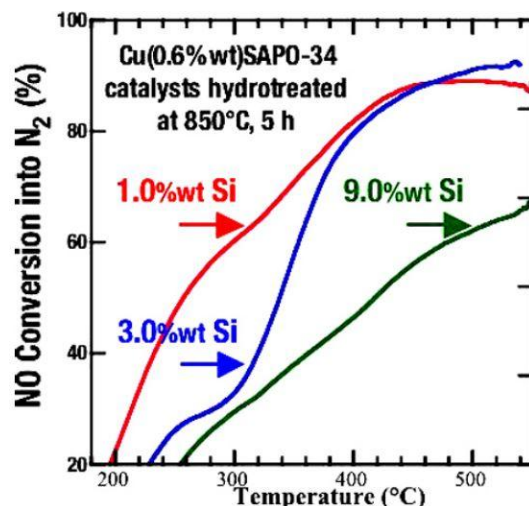
Figure 2.3-2: Reaction temperature dependence of NO_x conversion over Cu/SAPO-34 catalysts with various Si contents [62].

While preparing (hydrothermal synthesis) potential samples, the impact of Si content on the stability and the NH_3-SCR activity has been thoroughly investigated (**Fig. 2.3-2.**). It has been found that Cu/SAPO-34 with only 1.0-1.2 wt% of Si exhibits superior performance in terms of both stability and SCR activity in a temperature range between 200 and 550°C under H_2O conditions, compared to samples with high Si content [62].

2.4. SCR Catalytic Activity

A direct relationship between preparation method and SCR activity is suggested to be a challenge, while the NO_x reduction and NH_3 oxidation rates are mainly correlated to the amount of metal ions (i.e. metal content or loading). The catalytic activity of metal ion-exchanged zeolites, in fact, varies from one catalyst to another. Several determining factors which are considered to have impact on the catalytic activity are the

- zeolite structure,
- type of metal ions,
- ion exchange degree,
- Si/Al ratio,
- temperature range, and
- identity of active sites.

The deNO$_x$ activity and NH_3 oxidation ability can, therefore, vary among catalysts that consist of the same framework type (e.g. small pores) and are ion-exchanged with the same metal (i.e. type of metal ions), but with different metal loadings (i.e. ion exchange degree) [26].

2.4.1. *Influence of Metal Content on NH₃-SCR and NH₃ Oxidation*

It is suggested that ion-exchanged catalysts contain several different active sites. At low metal contents, studies reveal that the metal is mostly located in isolated mononuclear (monomeric) sites, leading to increased SCR activity and NO_x conversion. At high metal contents, both mononuclear and higher clustered species (oligomers) are detected, while the percentage of isolated sites decreases. At an even higher loading, clusters are formed probably by partial breakdown of the zeolite lattice (**Fig. 2.4.**) [30, 63].

At high exchange levels the SCR activity is increased below 300°C, but it is decreased at higher temperatures. The metal oxide particles formed at high aging temperatures obstruct the pores of the zeolite framework, leading to decreased NH_3-SCR activity and enhanced NH_3 oxidation ability (with oxygen migration over active sites) [26, 63].
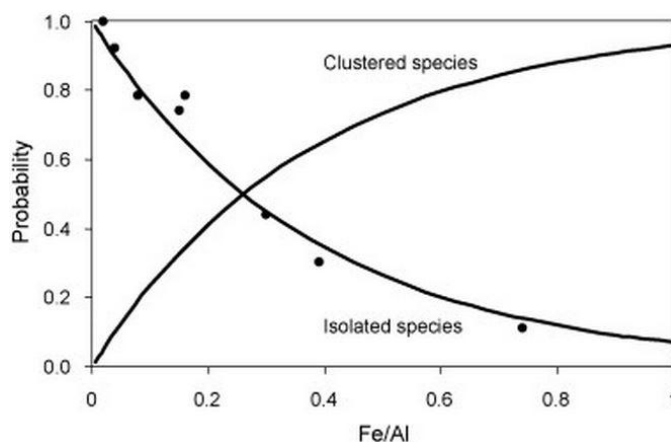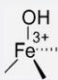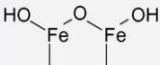

Figure 2.4: Probabilities P$_{isol}$ and P$_{clust}$=1-P$_{isol}$ for forming isolated and clustered species, respectively vs. Fe/Al for Fe/ZSM-5 catalysts with Si/Al=14 [30].

During the SCR of NO_x, further growth and restructuring of metal oxide clusters is observed. Clustering begins with lower clustered species (dimers) and is followed by others with different nuclearity. Therefore, dimers may be the second most prevalent species aside from monomeric species in the samples (**Table 1**). From the comparison of structural and catalytic properties of different catalysts, it is concluded that the SCR of NO_x by NH_3 is catalyzed by various entities such as mononuclear sites, oligomers and large particles [30, 55].

The NO_x conversion in the presence of O_2 or NO_2 over an ion-exchanged zeolite initially increases with temperature, then it reaches a conversion maximum around 300°C, and afterwards it declines. This decrease at high temperatures is attributed to NH_3 oxidation, competing with NO_x reduction [58]. Between 300°C and 400°C, higher clustered species (oligomers) contribute less to the SCR activity than lower clustered species (dimers). They also appear to cause the non-selective oxidation of NH_3 at higher temperatures [49]. Above 500°C, the deNO$_x$ efficiency is significantly reduced, while the NH_3 oxidation to N_2 and NO is enhanced. Both mononuclear sites and dimers are favourably active in the NO_x reduction, but oligomers and aggregated surfaces are more active in the non-selective NH_3 oxidation to N_2 and NO [30, 55, 63].

Table 1: Concentrations of monomeric, dimeric, clustered and oligomeric species in Fe/ZSM-5 measured by UV-vis spectroscopy [30, 55].

Fe/Al	Fe [wt.%]	Monomeric species [%] Fe^{3+}–OH	[a]	Clustered species (dimeric and oligomeric species) [%]	Dimeric species [%] HO–Fe–O–Fe–OH	Oligomeric species [%] $Fe_xO_y(OH)_z$ $x \geq 3$ [b]
0.02	0.14	95	100	5	4	1
0.04	0.27	90	92	10	8	2
0.08	0.56	79	78	21	15	6
0.15	1	68	74	32	18	14
0.16	1.1	66	78	34	18	16
0.3	2	46	44	54	16	38
0.39	2.6	37	30	63	13	50
0.45	3	31	–	69	11	58
0.74	5	15	11	85	4	81

[a] Measured by UV–vis spectroscopy. Sub-bands at $\lambda \leq 290$ nm.
[b] Difference between the concentration of clustered and dimeric species.

A rise in concentration of clustered sites owing to higher metal loading facilitates NH_3 oxidation, and partial NH_3 oxidation may occur on Fe- or Cu- highly exchanged catalysts. For instance, it is found that high Fe loading, low Si/Al ratio and low NH_3 concentration are favourable for NH_3 oxidation to N_2 over various Fe-zeolites [26, 59].

The metal content is directly related to the stability of single metal sites in exchange positions. Metal ions in zeolites with a low ion exchange degree (less aggregation) or a high Si/Al ratio seem to have little interaction with each other, because it is unlikely for two metal ions to be too close. Accordingly, such metal ions are more stable than those in highly exchanged zeolites where the ions are very interactive. This fact applies to an increased Cu content case, which results in lower hydrothermal stability (and severe hydrothermal deactivation) e.g. for Cu/ZSM-5 catalyst in urea-SCR [64].

Similarly, with further introduction of copper in Cu/SAPO-34 there is a decline in SCR activity. This is perhaps due to the replacement in Si-OH-Al by Cu^{2+} ions that inhibit the adsorption, storage and migration of NH_3 in the SCR reactions. Moreover, excessive Cu loading probably is the predominant reason for worsening of the hydrothermal stability of Cu/SAPO-34 catalysts [36, 39, 40, 43, 62].

3. EXPERIMENTAL PART

This section provides a description of which materials were prepared, how the used methods or techniques were carried out, and how the data were collected, so that it allows for the reproducibility of the procedure as well as the evaluation of this work.

3.1. Catalyst Synthesis and Characterization

In this work, Cu ion-exchanged silico-aluminophosphate (SAPO) catalysts with two different Cu loadings were prepared. Initially, SAPO-34 zeolite was prepared using the procedure of hydrothermal synthesis and aging with the following *mol* compositions: *Al_2O_3 : 1.06 P_2O_5 : 1.08 SiO_2 : 2.09 Morpholine : 66 H_2O.* The prepared zeolites were then ion-exchanged in two consecutive stages with NH_4NO_3 solution and one stage with various concentrations of copper nitrate solution.

3.1.1. Synthesis of SAPO-34 Zeolite

- In the first step, a solution of orthophosphoric acid H_3PO_4 (85 wt%, Merck) dissolved in MilliQ water was prepared and constantly stirred for over 15 min at room temperature.
- Then pseudoboehmite (74% Al_2O_3, PURAL SB-1, Sasol) was spoonwise added within 2 h to the diluted orthophosphoric acid solution. Continuous stirring was carried out at room temperature for 12 h, until a uniform gel was obtained.
- In the next step, a homogeneous solution of colloidal silica SiO_2 (40 wt% in H_2O, LUDOX AS-40, Aldrich) and morpholine (tetrahydro-1,4-oxazine, Sigma-Aldrich) was prepared, and the silica - morpholine mixture was slowly added within 1h to the P-containing solution under constant stirring at room temperature.
- Afterwards, the slurry was continuously stirred at ambient conditions for 7 h, in order to become completely smooth and homogeneous.

3.1.2. Aging of SAPO-34 Zeolite

- The obtained mixture was first subjected to aging without stirring at room temperature for 24 h. The solution was then transferred and sealed into a 250 mL Teflon-lined stainless steel autoclave and heated at 200°C for 72 h.
- Crystallization was realized under autogenic pressure without stirring. The crystallization period started from the beginning of heating until the (pre-heated) autoclave reached temperature of 200°C.
- After cooling to room temperature, the liquid phase was separated from the solid phase by centrifugation. During this step, the crystalline mixture was thoroughly washed with MilliQ water several times and put into Teflon-lined autoclave at 100°C for 12 h to dry.
- Finally, the resulting product was ground into fine powder and thereafter calcined at 550°C for 6 h with a ramping rate of 5°C min^{-1} and left to cool naturally.

3.1.3. Synthesis of Cu/SAPO-34 by Wet Ion Exchange

The procedure of synthesis of Cu/SAPO-34 by WIE consisted of two main stages, in order to introduce a controlled amount of Cu ions to the zeolite catalysts. The naming convention, which was deployed in this thesis for each catalyst, was based on the molarity of the copper nitrate solution used in the synthesis process, i.e. 0.05 and 0.8 M.

Ammonium nitrate, NH_4NO_3, exchange (two times, same procedure, one molarity: 5.4 M)

Copper nitrate, $Cu(NO_3)_2$, exchange (one time, same procedure, two molarities: 0.05 M & 0.8 M)

1st stage: NH_4NO_3 exchange

- The NH_4-form of SAPO-34 zeolite was prepared by exchanging with a 5.4 M solution of NH_4NO_3 (99%, Sigma-Aldrich), adding MilliQ water and stirring until homogeneous at room temperature. The ratio of NH_4NO_3 solution volume to mass of zeolite was 7:1, where volume and mass were measured in mL and g, respectively. This means that for the ion exchange of 1 g zeolite, 7 mL NH_4NO_3 were used.
- Then zeolite SAPO-34 fine powder was added into the agitating solution at room temperature. This was done spoonwise and not directly, in order to avoid lowering the pH too fast. However, because the pH of the solution was quickly decreasing, some drops of 2 M diluted ammonium hydroxide (NH_4OH) solution were accordingly added to increase the pH again.
- It is worth noting that, in the 2nd time during the addition of zeolite, the pH of solution was not decreasing as fast as in the 1st time, and so pH adjustment was rarely needed. However when adding NH_4OH drops, special attention was paid to adjust the pH in the range of 3.0-3.5. Lower pH could cause the structure of zeolite to be damaged or broken, and higher pH could induce formation of *precipitate* of ammonium salt.
- After all SAPO-34 zeolite powder was added, the solution was kept under stirring until the pH was stabilized around 3.4-3.5. The solution was then heated in "oil bath" to approximately 80°C, which was maintained as constant as possible. During heating, the pH of the solution decreased, and when it reached 3.0 more drops of diluted NH_4OH solution were added in order to keep the pH in the 3.0-3.5 interval.
- When temperature was steady at 80°C, the slurry was maintained under agitation at 80°C for more than 1 h, with the pH being maintained relatively stable at 3.0-3.2 with few fluctuations (although it was initially changing). Afterwards, the slurry was left to cool until reaching room temperature.
- Centrifugation was then carried out several times to separate the solid phase from the liquid one. Each time, the slurry was decanted (i.e. poured gently from one container to another), especially without disturbing the powder sediment at the bottom, which was thereafter washed with MilliQ water to remove the residues (e.g. NH_4 precursor).
- The resulting support was finally dried at 100°C for 12 h, followed by another ion exchange process, described below.

2nd stage: Cu(NO$_3$)$_2$ exchange

For Cu ion exchange in the ammonium-form of the zeolite, where Cu ions were introduced to the zeolite cavities, two solutions of Cu(NO$_3$)$_2$ (98%, Alfa Aesar GmbH) were used as precursors. Hence, two Cu/SAPO-34 solutions with molarities 0.05 M and 0.8 M were prepared by adding Cu(NO$_3$)$_2$ in MilliQ water. The ratio of volume of Cu(NO$_3$)$_2$ solution to mass of zeolite was 4:1, where volume and mass were measured in mL and g, respectively.

- For Cu(NO$_3$)$_2$ of 0.05 M, the pH of the solution was initially around 4, while for 0.8 M it was about 2.3. For 0.05 M, when the solution was heated to 70°C in "oil bath", the pH was adjusted within a range of 3.5-4.0 without any NH$_4$OH needed to increase it further. By contrast, for 0.8 M the pH decreased to 2.1 during the heating process. By adding lots of drops of NH$_4$OH, there was a risk to provoke *precipitation*, but it was still clear in the appearance.
- When the temperature was stabilized at 70°C with small fluctuations in "oil bath", and the pH was raised enough (pH~2.6 for 0.8 M), zeolite powder from the previous exchange process was carefully added spoonwise to the solutions. In the course of NH$_4$-zeolite addition, the pH was increased just to decrease again gradually (minimum pH~2.25 for 0.8 M).
- The zeolite solutions were then maintained under stirring at 70°C for more than 1 h. During the agitation, the pH was decreased but only down to 3.0 for 0.05 M, and down to 2.3 for 0.8 M. The pH adjustment using NH$_4$OH was needed to increase the pH, and special care was taken to prevent *precipitation* of the solution or breaking of the zeolite structure. Next, the solutions were left to cool to room temperature.
- Centrifugation was afterwards performed several times to separate the solid from the liquid phase. The resulting slurry was decanted without disturbing the powder sediment at the bottom, which was therein washed with MilliQ water to remove the residual Cu precursor.
- Then the obtained zeolite was dried at 90°C for 12 h to completely eliminate H$_2$O. At last, calcination of the powder was carried out at 550°C for 3 h with a ramping rate of 5°C min^{-1} followed by 750°C for 2 h with the same ramping rate.

The Cu/SAPO-34 catalysts were characterized by XRD to verify the CHA zeolite structure and crystallinity and then used for washcoating the monoliths. Lastly, they were studied thoroughly for NH$_3$-SCR and NO$_x$ reduction activity by flow reactor and micro-calorimeter experiments.

3.1.4. Catalyst Characterization

X-ray diffraction (XRD) is a common characterization technique owing to its speed and ease of use, deployed to study the bulk crystal structures and to determine the chemical phase composition of the catalysts. In addition, it only requires a small amount of catalyst sample and it is a non-destructive technique.

Crystals consist of parallel planes formed by repetitive arrangement of atoms in 3D space. These planes are separated from one another by distance (*d*), which varies according to the nature of the material. When X-rays are projected onto the crystalline

material, a diffraction pattern is produced, because their wavelength (λ) is typically the same order of magnitude (1-100 Å) as the spacing between planes in the crystal. For constructive interference from nearby crystallographic planes of the crystal lattice, the path difference between two beams with identical λ and phase must be equal to an integer (n) multiple of the λ of the radiation. This is known as *Bragg's law*:

$$n\lambda = 2d\ sin\theta$$

where *2d sinθ* is the path difference between two beams and *θ* is the scattering angle. A unique diffraction pattern is obtained, by measuring the intensity of scattered waves as a function of scattering angle. Within the crystal structure, the angles of diffraction differ for the various planes. When a mixture of different phases is present, the resulting pattern is a summation of the individual patterns.

In order to check the SAPO-34 structure as CHA type, by identifying the crystal phases, and to understand the quality of the catalysts tested, XRD measurements on the catalysts were conducted. This was done by utilizing a "Scintag X2" powder X-ray diffractometer equipped with a computer-controlled goniometer and an X-ray source with Co Ka radiation (λ = 1.78897 Å). Spectra were collected at scan-run *2θ* values of 5° to 40° using a step size of 0.02 °/s. The instrument sensitivity and resolution were high enough to accurately characterize the catalysts used in this work.

3.2. Monolith Preparation
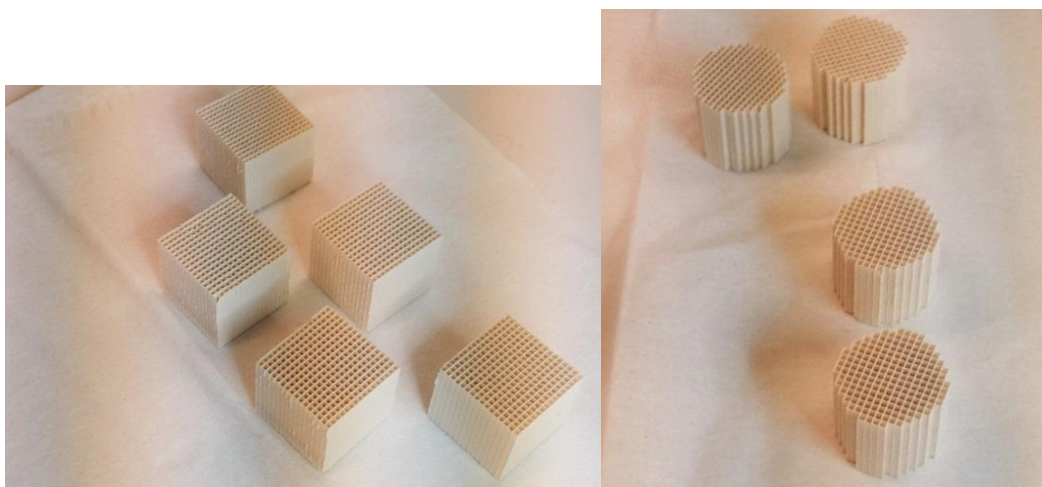
Figure 3.2: Photographs of cordierite monolith samples before (left) and after (right) their final shaping-cut.

- Initially, the monoliths were cut from a commercial honeycomb cordierite structure (20 mm in length, 21 mm in diameter, 400 cpsi) (**Fig. 3.2.**) and then calcined at 500°C for 2 h with a ramping rate of 5°C min^{-1}.
- In order to enhance the attachment of the catalysts, the monolith substrates were washcoated with a thin layer of "binder". This was done with alumina by immersing and drying the monoliths a few times in a mixture containing 95 wt% liquid phase (equal amounts of ethanol and MilliQ water, 1:1) and 5 wt% solid phase of boehmite (Disperal

D, Sasol, Gmbh). This washcoating was followed by drying at 90°C hot air for 2 min. Thereafter, the alumina-coated monoliths were calcined at 500°C for 2 h with a temperature ramping rate of 5°C min^{-1}.

- After cooling to room temperature, a procedure of 0.05 M and 0.8 M Cu impregnation in Cu/SAPO-34 catalysts took place. For these impregnations, two slurries were used both consisting of 20 wt% solid phase of catalyst/boehmite and 80 wt% liquid phase of ethanol and MilliQ water (1:1). The Cu/SAPO-34 and boehmite mass ratio in solid phase was 95:5 based on weight. In this thesis, a significantly thinner washcoat of Cu/SAPO-34 catalysts, compared to commercial catalysts, was used in order to minimize the mass transfer.

- Each time after dipping the monoliths, the excess slurry was removed and the monoliths were dried for 2 min at 90°C hot air. The procedure was repeated a few times until the desired amount of washcoat (~500 mg) was reached. Afterwards, the coated monoliths were calcined at 550°C for 2 h with the same ramping rate.

3.3. Ash Deposition

The two Cu/SAPO-34 washcoated monoliths were then coated with ash from renovated filters, provided by Volvo Cars. Ash powder in two different concentrations was deposited (**Fig. 3.3.**) on the Cu/SAPO-34 samples with 0.05 M and 0.8 M Cu loadings. Concentrations of 2.5 g/L and 5 g/L ash, corresponding to 17.5 mg and 35 mg ash, respectively, were employed and thus required to be attached on the previously prepared samples. The rest of the calcined monoliths remained "pure" and were used as references or benchmarks. Additionally, surfactant-washcoated monoliths were tested just for comparison with flow reactor experiments.

Figure 3.3: Photograph of monolith samples after ash coverage by washcoating.

A mixture of ash powder and ethanol was prepared and the obtained mixture was impregnated to the monoliths at room temperature, under control of the monoliths weight. The ash based monoliths were dried at room temperature for about 1 h. The 0.05 M and 0.8 M Cu/SAPO-34 based monoliths and the ash based monoliths (not calcined) were used on the flow reactor measurements. During the micro-calorimeter experiments that were also performed in this work, an amount of ~100 mg ash powder was loaded into the reactor micro-tube, as described below (see **3.5.**).

3.4. Flow Reactor Experiments

The coated monoliths were tested for *"standard NH₃-SCR"* activity measurements which were carried out in a flow reactor system. Particularly, each monolith was wrapped in fine quartz wool to ensure there was no gas leakage around the sample. Then it was loaded into a horizontally-aligned quartz reactor tube, which was 800 mm in length and 22 mm in inner diameter, operating at atmospheric pressure.

Two K-type thermocouples were inserted into monolith central channels, such that the one would be positioned about 1 cm in front of the monolith to measure the reactor gas temperature, whereas the other would stay inside the channel to show the catalyst-bed temperature. The former thermocouple was fitted so as to minimize the effect of any exothermic or endothermic catalytic reactions on the temperature controller. LabVIEW^{TM} program was used to steer and monitor the temperature and the gas flows during the experiments. A heating coil was twined around the tube, as seen in **Fig. 3.4-1.**, and proper insulation enwrapped it to prevent significant heat loss.
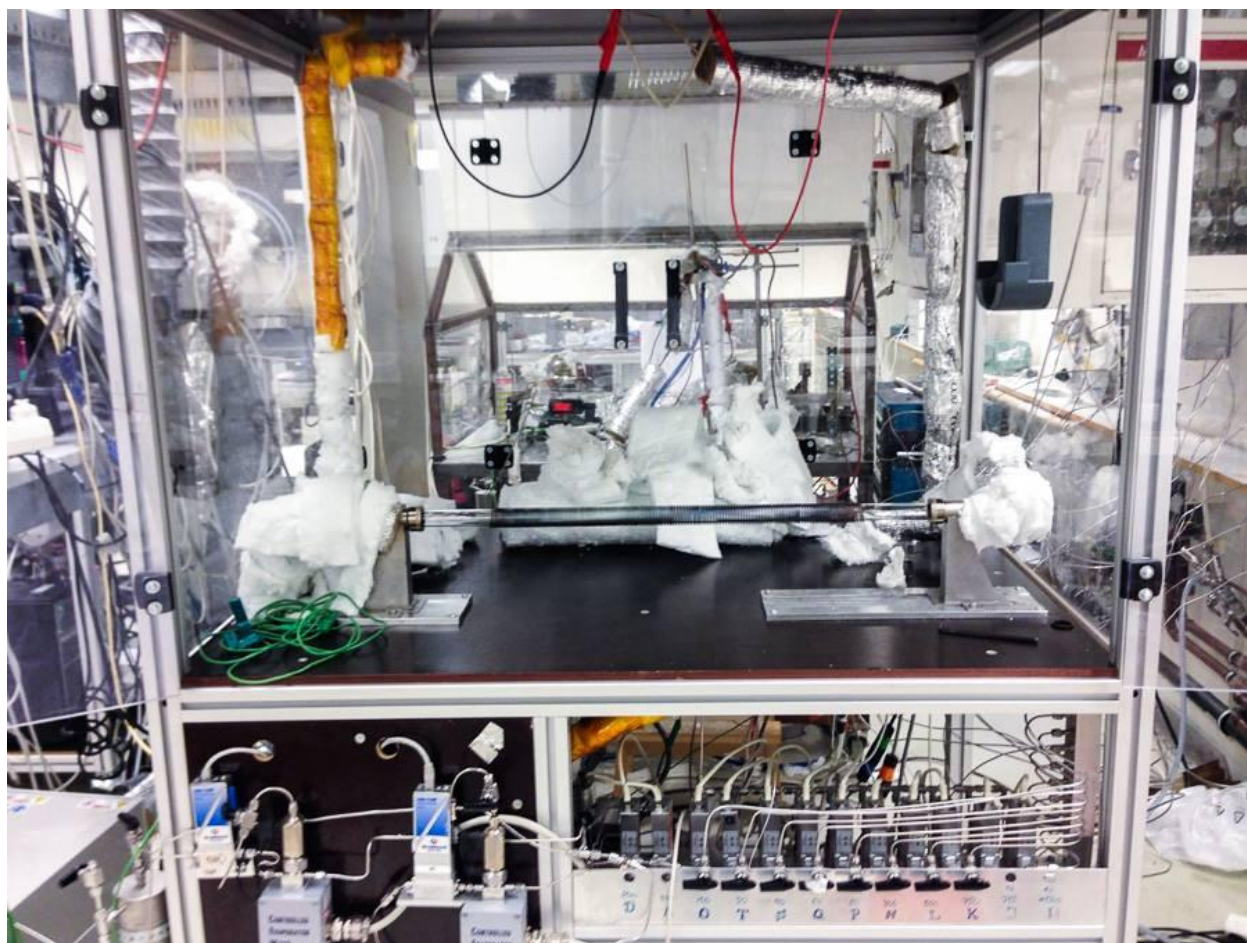

Figure 3.4-1: Photograph of the MFCs and CEM systems in the flow reactor setup.

31

Bronkhorst® High-Tech mass flow controllers (MFCs) and controlled evaporation and mixing (CEM) systems were used to regulate the inlet feed gases and the water stream flow, respectively. The MFCs allowed a wide range of feed gas concentrations, compositions and flow rates of the reaction gas mixture to be explored (**Fig. 3.4-2.**).
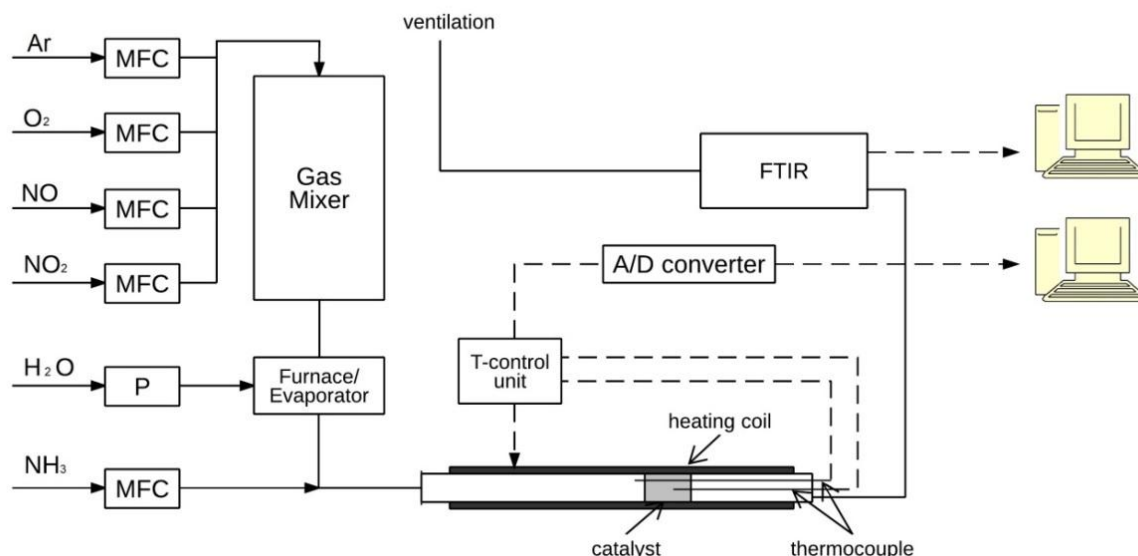
Figure 3.4-2: Schematic of the flow reactor setup, comprising of its different constituents.

The reactor system was directly connected to a Fourier transform infrared (FTIR) spectrometer (MKS MultiGas^{TM} 2030) to analyse the outlet gaseous products, which were NH_3, NO, NO_2, N_2O and H_2O in most cases. The inlet and the outlet lines were heated to 200°C to prevent the deposition of ammonium nitrate during the experiments.

3.4.1. _FTIR Imaging Analysis_

Fourier transform infrared (FTIR) imaging is the main analytical technique used in these studies. The MKS MultiGas^{TM} 2030 is an FTIR-based gas analyser designed to monitor automotive exhaust gases at 1 Hz frequency. It allows gas flows up to an exceeding 100 L min^{-1} with no back-pressure or acoustic noise generated, that could degrade the quantitative measurements. It is able to simultaneously quantify many gases at that frequency. Samples containing up to 30% H_2O can be monitored by maintaining the gas temperature and PM filtration. Detection limits of ≤1 ppm are achievable with this analyser by using high sensitivity and narrow-range detectors.

The FTIR spectrometer therein is able to reach a high speed of 0.5 cm^{-1}. Upon exiting the spectrometer, the IR light beam is focused by lenses to impinge on the detectors, allowing the gaseous products to be analysed in parallel. The analyser incorporates a liquid-nitrogen-cooled detector that can keep cryogenic temperatures for up to 12 h. The entire system is complete with software.

3.4.2. Reaction Conditions

The line used for H_2O injection into the CEM system was heated to a temperature greater than the boiling point of water; in these experiments, it was heated to 150°C. The carrier gas passed through the CEM to mix with H_2O steam, and the combined gas feed continued through heat-traced lines to the reactor inlet. The entire setup was completely heat-traced in order to prevent

- H_2O condensation,
- deposition of ammonium nitrate during the experiments.

The system was operated at 3000 mL min^{-1} total gas flow, corresponding to a gas hourly space velocity (GHSV) of 26000 h^{-1}. Prior to the experiments, NH_3, NO, NO_2 and N_2O gases were calibrated in the empty reactor tube with known concentrations at 200°C.

Prior to each experimental sequence, each monolith was pretreated to 500°C in Ar with a temperature ramping rate of 10°C min^{-1}, and subsequently the same temperature was held for 20 min in order to remove residual species adsorbed on the surface (to achieve clean surface area). Notably, for the ash-coated monoliths, an additional pretreatment was performed by heating the samples at 400°C, followed by their exposure to 8% O_2 at 400°C for 60 min, in order to remove the possible ethanol traces, during the ash deposition procedure, from the samples used.

After pretreatment, the monoliths were exposed to *"standard SCR"* conditions with 8% O_2, 5% H_2O, 400 ppm NH_3 and 400 ppm NO. Ar was used as the inert balance gas over the catalysts, in order to obtain a stable catalytic behavior during measurements. All NH_3-SCR of NO_x experiments were carried out within a temperature range of 150°C to 700°C by increasing the temperature stepwise (150, 175, 200, 225, 250, 300, 350, 400, 450, 500, 550, 600, 650, 700°C) with 5°C min^{-1} between each step.

The NH_3-SCR tests for the fresh samples and the samples coated with ash were carried out under the same experimental sequence to allow for comparison. Only the intermediate test for Cu/SAPO-34 coated with ethanol took place in the range of 150-500°C instead. Except for this experiment, all flow reactor measurements were realized for both 0.05 M Cu and 0.8 M Cu concentrations of Cu/SAPO-34 samples with and without ash coverage. This ash coating effect was investigated for both 5 and 2.5 gL^{-1} ash (meaning 35 and 17.5 mg ash, respectively).

3.5. Micro-calorimeter Experiments

Two quartz micro-tubes were mounted inside the DSC, as shown in **Fig. 3.5.** The one served as sample holder where an amount of 100 mg ash powder was placed on a sintered quartz bed, and the other served as reference. Prior to each experiment, the surface of the quartz bed was treated by exposure to Ar at 500°C for approximately 45 min, to become as clean as possible and allow for reuse. The outlet gases were measured by the MS, which detected masses of 2-hydrogen, 17-ammonia, 18-water, 20-argon, 30-nitrogen oxide and 32-oxygen. All micro-calorimetric measurements were performed using the micro-calorimeter setup, as depicted in **Fig. 3.5.**, which consisted of three different instruments:

- a "Setaram Sensys" differential scanning calorimeter (DSC) for heating and thermal analysis of the samples,
- several mass flow controllers (MFCs) for feeding and mixing the inlet gases, and
- a "Hiden HPR-20 QUI" mass spectrometer (MS) for measuring the outlet gas concentration.
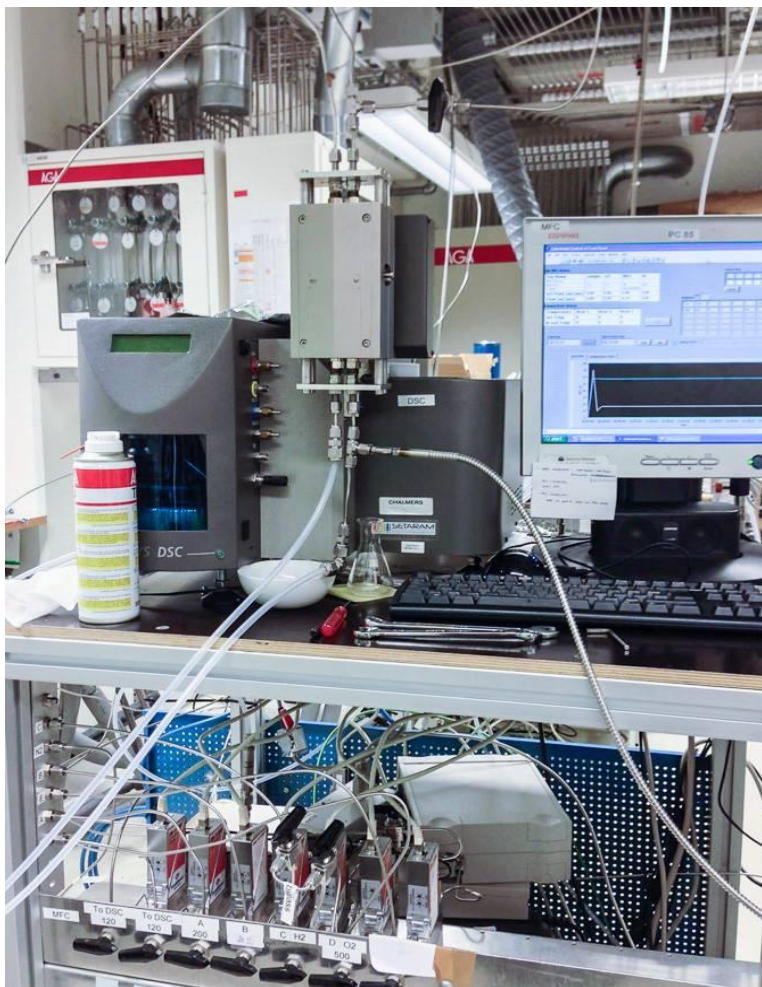
Figure 3.5: Photograph of the DSC, MFCs and MS systems for the micro-calorimeter experiments.

A total gas flow of 20 mL min^{-1} was used for the ash exposure to gases, while the remaining gas flow was sent to the ventilation system. Ar acted as inert balance gas for all sequential experiments conducted when using the micro-calorimeter setup, as described below.

- *NH$_3$-TPD* experiment was conducted in order to investigate the NH$_3$ storage of the ash sample at 50°C. The sample was exposed to 200 ppm NH$_3$ for 2 h. After flushing with Ar for 30 min, the temperature was raised to 800°C with a ramping rate of 10°C min^{-1}.
- *NO-TPD* experiment was performed to study the NO storage of the ash sample at 50°C and the ash powder was exposed to 200 ppm NO for 2 h, followed by Ar only for 30 min before the temperature was increased up to 800°C with a ramping rate of 10°C min^{-1}.

- *NO$_2$-TPD* experiment was performed to examine the NO$_2$ storage of the sample at 50°C and 200 ppm NO$_2$ for 2 h were used. Afterwards, the same procedure was followed for this experiment as for either NH$_3$- or NO- TPD experiment.
- *NH$_3$ oxidation* experiment was also carried out, where the sample was treated with 500 ppm NH$_3$ and 8% O$_2$ for 3 h. The temperature was increased from 50°C up to 700°C in the same gas mixture (O$_2$, NH$_3$, and balanced Ar) with a ramping rate of 5°C min^{-1}.

It is worth noting that since each procedure was performed using ash, special care was taken for appropriate removal of ash and cleaning of the micro-tube between the experiments. Moreover, for each of the discussed experiments, a new ash sample was used to determine the adsorption and desorption, and the coverage-dependent heat or activation energy.

3.6. Ash Composition Analysis

Lastly, an *Inductively Coupled Plasma-Sector Field Mass Spectrometry* (ICP-SFMS) analysis of the ash powder sample was performed by ALS Scandinavia AB to gather information for the elemental composition and contents (for example S, Zn, Fe, Cu, Ni, Cr, Zr and Pt) of the ash, as well as examining if there were any impurities. The obtained analysis served well the quantification of the ash content in terms of its composition and, accordingly, the interpretation of the findings in this master thesis.

4. RESULTS AND DISCUSSION

In this section, all of our findings which were obtained through research in this work, along with their respective analysis and discussion, are presented. The discussion is supported by references when necessary to add to their validity.

4.1. Catalyst Characterization

The XRD analysis is used to characterize the catalysts and understand their quality and is conducted for Cu/SAPO-34 of 0.05 M, Cu/SAPO-34 of 0.8 M and SAPO-34 only, right after their synthesis. The results are presented in **Fig. 4.1.**, and they clearly show that the CHA structure type is maintained in Cu/SAPO-34 zeolite catalysts, despite the very low pH during the ion exchange process [65].
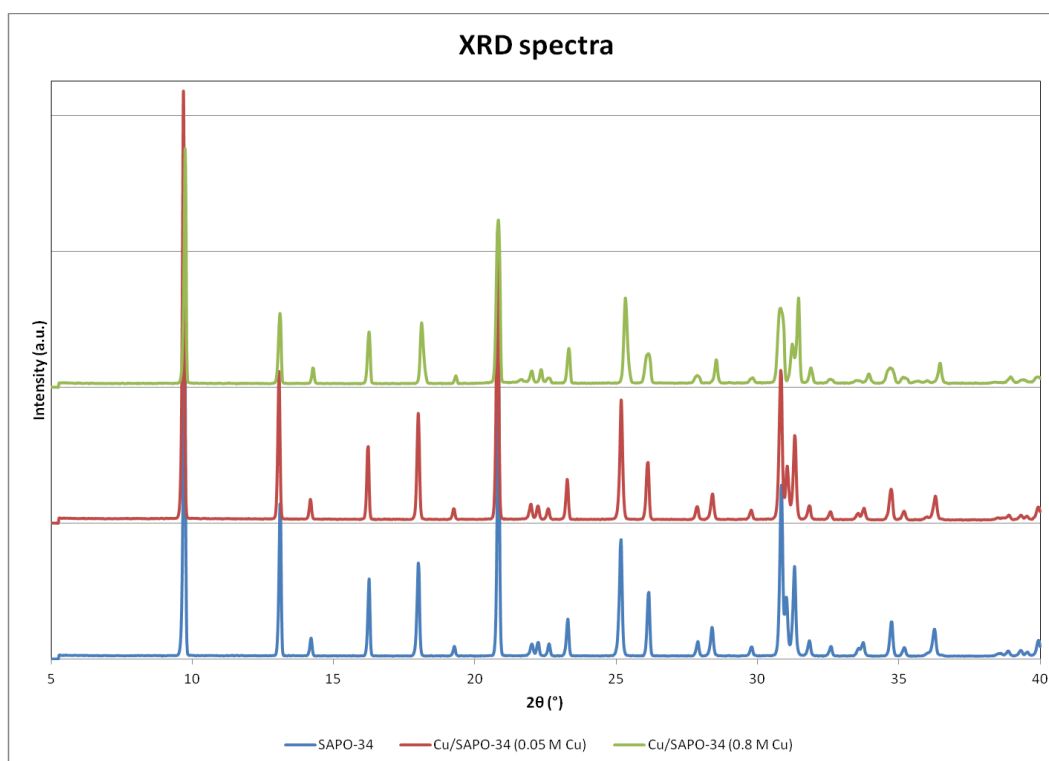
Figure 4.1: XRD patterns for synthesized 0.05 M Cu/SAPO-34, 0.8 M Cu/SAPO-34 and unsupported SAPO-34 samples.

The obtained diffraction spectrum (**Fig. 4.1.**) is deployed to verify the structure and crystallinity of Cu/SAPO-34, and is very useful. The peaks confirm the presence of the SAPO-34 structure, by comparison with the existing database.

4.2. Calibration of Gases

Gas calibration of the flow reactor equipped with the FTIR imaging system is employed to correct the measurements for NH_3, CO, CO_2, N_2O, NO and NO_2 gases. This procedure provides the acquired data with validation, since the calibration curves for all gases are lines (3rd degree polynomial approximation) with R^2 value of 1 or ~0.9999. These calibration plots present the predicted concentration of each gas in *ppm* as a function of the measured concentration in *ppm* received by the actual FTIR signal. Therefore, known concentrations are used to establish the calibration model of measured concentrations. By this method, all gas calibrations are accurate and readily used for the gases produced during the reactions.

4.3. Study I - Effect of Cu Loading on Fresh Samples

The influence of a low Cu content in comparison to a higher Cu content of fresh Cu/SAPO-34 samples on the *"standard NH_3-SCR"* activity and NO_x conversion is shown in **Fig. 4.3-1.** and **Fig. 4.3-2.**, respectively. The results from the steady-state concentrations of NH_3 and NO_x are depicted. A stepwise temperature increase from 150 up to 700°C comprises the reaction temperature range. The Cu/SAPO-34 catalysts are exposed to a gas mixture that consists of 400 ppm NO, 400 ppm NH_3, 8% O_2 and 5% H_2O. The fresh Cu/SAPO-34 catalysts show consistency in results with the *"standard SCR"*, where approximately similar amounts of NH_3 and NO_x are consumed during the reaction, which can be seen when comparing the results in **Fig. 4.3-1.** and **Fig. 4.3-2.** below.
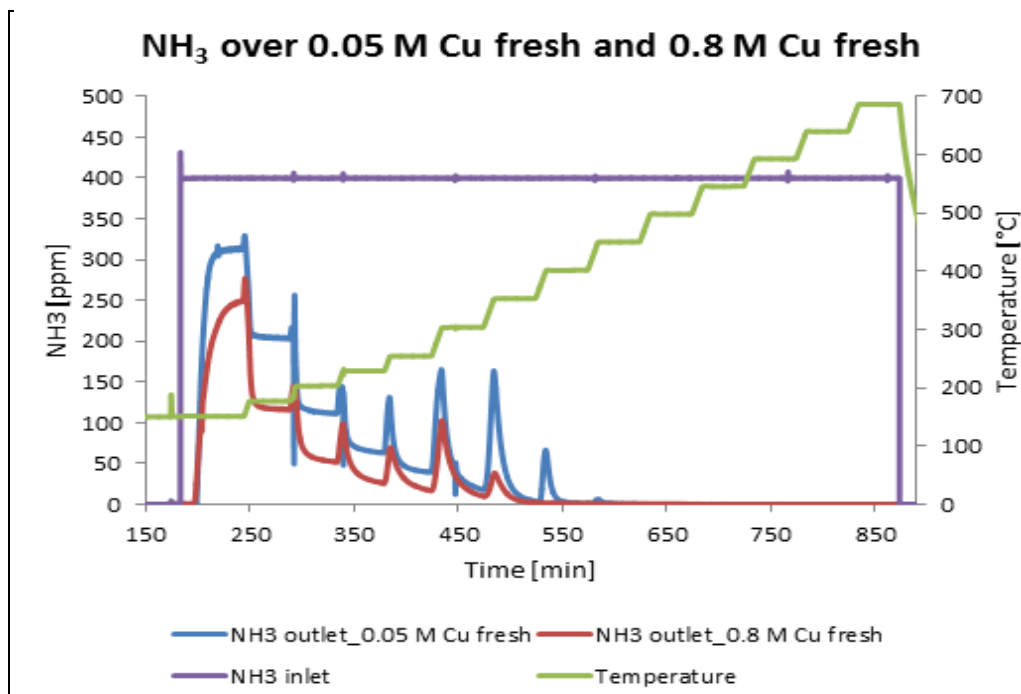
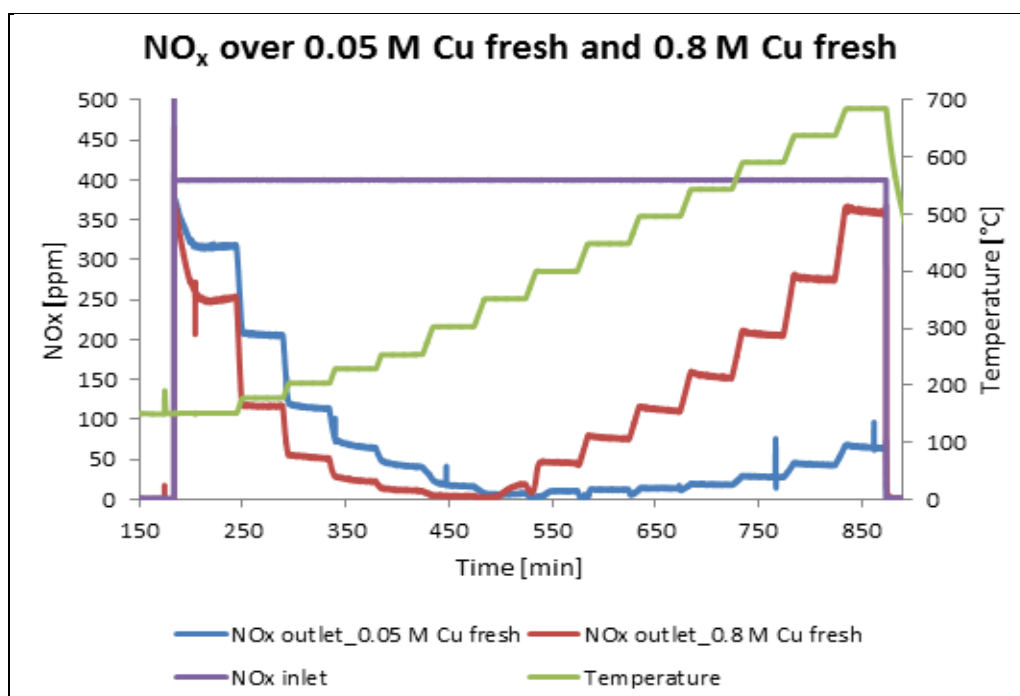**Figure 4.3-1: NH₃-SCR activity comparison between fresh 0.05 M Cu/SAPO-34 and fresh 0.8 M Cu/SAPO-34.**

In fact, superior NO_x and NH_3 conversions for the 0.8 M Cu/SAPO-34 sample at low temperatures (150-300°C) are seen. A total NH_3 conversion at high temperatures (>400°C) is presented in **Fig. 4.3-1.**, since NH_3 reacts with NO_x and O_2 during *"standard SCR"* reaction in combination with ammonia oxidation.

Furthermore, as seen in **Fig. 4.3-2.**, NO_x conversion is higher for the Cu/SAPO-34 with higher copper loading at low temperatures, but above 350°C the results are opposite. A remarkable decrease (worsening) in NO_x reduction activity with increasing temperature is seen above 350°C due to NH_3 oxidation. NH_3 oxidation takes place at such temperatures, and it is well-known that it acts counteractively to the NO_x reduction at high temperatures. The reaction **$4NH_3 + 3O_2 \rightarrow 2N_2 + 6H_2O$** (9) with oxygen (see also Theory section) for NH_3 oxidation thus occurs.

The impact of the Cu loading on the NO_x performance for fresh Cu/SAPO-34 samples is clearly observed. Apparently, NH_3 oxidation is larger on 0.8 M Cu-loaded sample compared to 0.05 M Cu/SAPO-34, which results in significantly lower NO_x reduction at high temperatures for the highly Cu-loaded sample. These results are consistent with the results for Cu/BEA found by Mihai et al. [66].

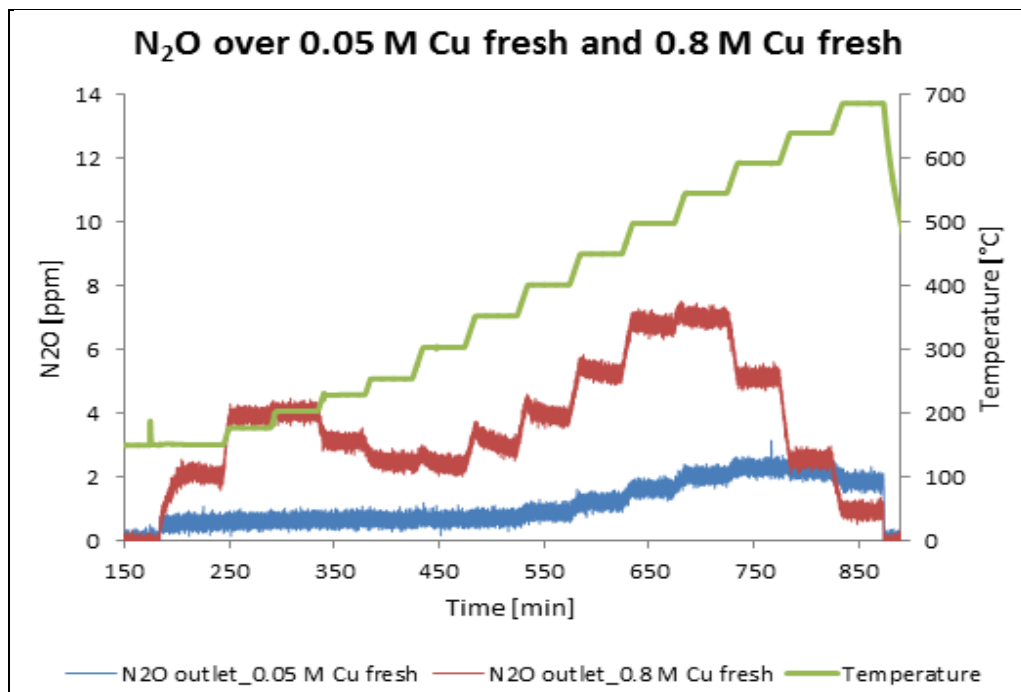**Figure 4.3-2: NO_x reduction activity comparison between fresh 0.05 M Cu/SAPO-34 and fresh 0.8 M Cu/SAPO-34.**

It has been previously observed that Cu/SAPO-34 possesses higher NO_x and NH_3 conversions in comparison to SAPO-34 support (H-form of SAPO-34), emphasizing the important role of Cu on the catalytic activity [40, 67]. The outstanding NH_3-SCR activity of Cu/SAPO-34 catalysts can be strongly determined by the states of isolated Cu^{2+} species located at the exchange sites of SAPO-34 microporous framework [39, 40].

4.3.1. Production of N₂O over Fresh Samples

Formation of some nitrous oxide (N_2O) is detected, and the production of various amounts of N_2O for the different catalysts is observed in the whole temperature range (**Fig. 4.3-3.**). However, there is a first maximum of N_2O concentration around 200°C and a second maximum at 550°C for the catalyst with high Cu content (0.8 M Cu/SAPO-34).

- The first maximum of just 4 ppm (low-temperature N_2O production) could be justified considering that, at low temperatures the quick thermal decomposition of NH_3-NO species, possible precursors for ammonium nitrate, gives N_2O as a product [68]. Particularly, when NH_3 and NO_2 are fed into the reactor, ammonium nitrate is formed according to the reaction (12) (see Theory section), where the NH_4NO_3 in the NO_x feed contains N_2O. Hence, this reaction can be rewritten as:
$$2NH_3 + 2NO_2 \rightarrow N_2O + N_2 + 3H_2O \ (14) \ [45].$$
- As for the second maximum of N_2O concentration (high-temperature N_2O production), at high temperatures undesirable oxidising properties of the SCR catalysts may arise, such that NH_3 is consumed by oxygen and additional NO or N_2O is formed. As shown in **Fig. 4.3-3.**, the N_2O amount of around 7 ppm is produced.

These side reactions that are in competition with the intended reactions either yield secondary emissions leading to unwanted N_2O or excess NO, according to the reaction (10) (see Theory section), or consume NH_3 unproductively [27, 28].

Figure 4.3-3: N₂O concentration comparison between fresh 0.05 M Cu/SAPO-34 and fresh 0.8 M Cu/SAPO-34.

Eventually, the deNO$_x$ activity of the catalysts and the N$_2$O production in NH$_3$-SCR reactions is temperature dependent and NO$_2$/NO$_x$ feed ratio dependent [45]. Like all metal ion-exchanged zeolites, various co-cations could play an important role in optimization of Cu/SAPO-34 catalyst or elimination of the undesirable formation of N$_2$O. Blocking some zeolite cavities by using co-cations, the system could be active at lower temperatures (~150°C) and could avoid the formation of N$_2$O [61].

But unlike other Cu-based zeolite catalysts, such as Cu/ZSM-5, Cu/BEA and Cu/FAU, studies show that the Cu/SAPO-34 catalysts only produce trace amounts of N$_2$O, which is less than 12 ppm for the entire range of reaction temperatures in this work, indicating excellent N$_2$ selectivity of the fresh Cu/SAPO-34 catalysts [40].

4.4. Study II - Effect of Cu Loading on Samples with Ash (5 g/L)

The NH$_3$ concentrations for the two different Cu/SAPO-34 samples after ash loading are depicted in **Fig. 4.4-1.** The general trends between the samples coated with ash (5 g/L) and the fresh samples (see **Fig. 4.3-1.**) are similar. However, the absolute concentrations are different with and without ash. The increasing of Cu content from 0.05 M to 0.8 M leads to the rise of NH$_3$ conversion (from a maximum of 300 ppm to 250 ppm NH$_3$).
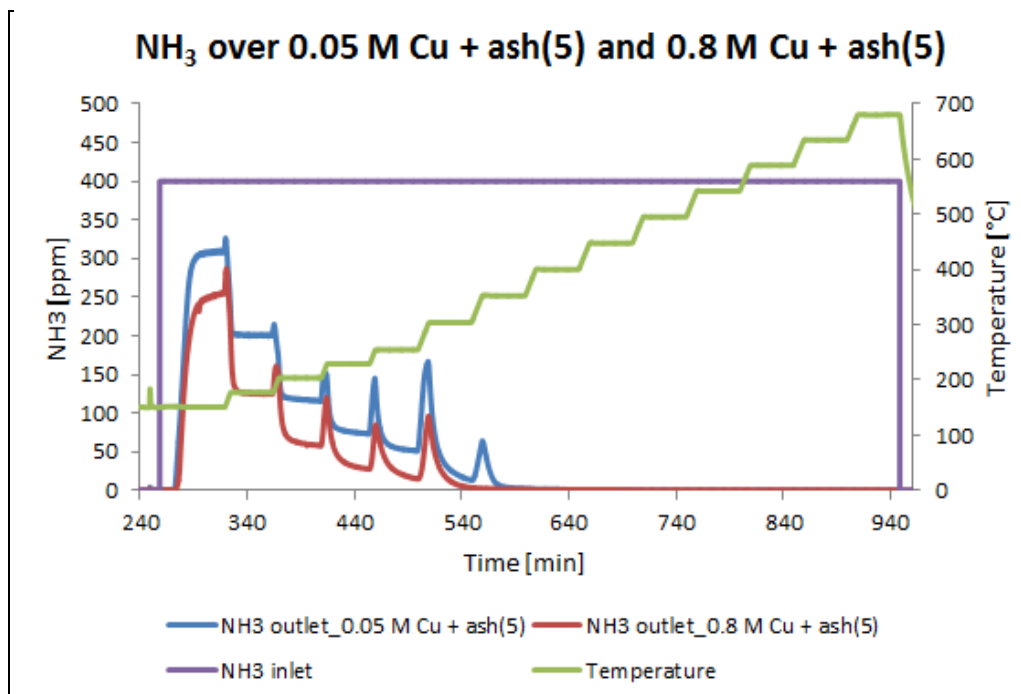
Figure 4.4-1: NH$_3$-SCR activity comparison between 0.05 M Cu/SAPO-34 with 5 g/L ash and 0.8 M Cu/SAPO-34 with 5 g/L ash.

As seen in **Fig. 4.4-2.** with increase in reaction temperature, the outlet NO_x concentration initially decreases, as anticipated. But when the temperature is higher than the optimum SCR reaction temperature, the outlet NO_x concentration begins to rise. As temperature keeps being raised, above 300°C the NO_x outlet gets higher for ash-loaded samples, a few times higher than the NO_x outlet over the fresh catalysts (**Fig. 4.3-2.**) [69]. However, it is worth noting that for samples with ash (**Fig. 4.4-2.**) the aforementioned decrease in NO_x conversion appears on both high and low Cu-containing samples in contrast to what is observed on the fresh samples without ash at high temperatures (**Fig. 4.3-2.**).
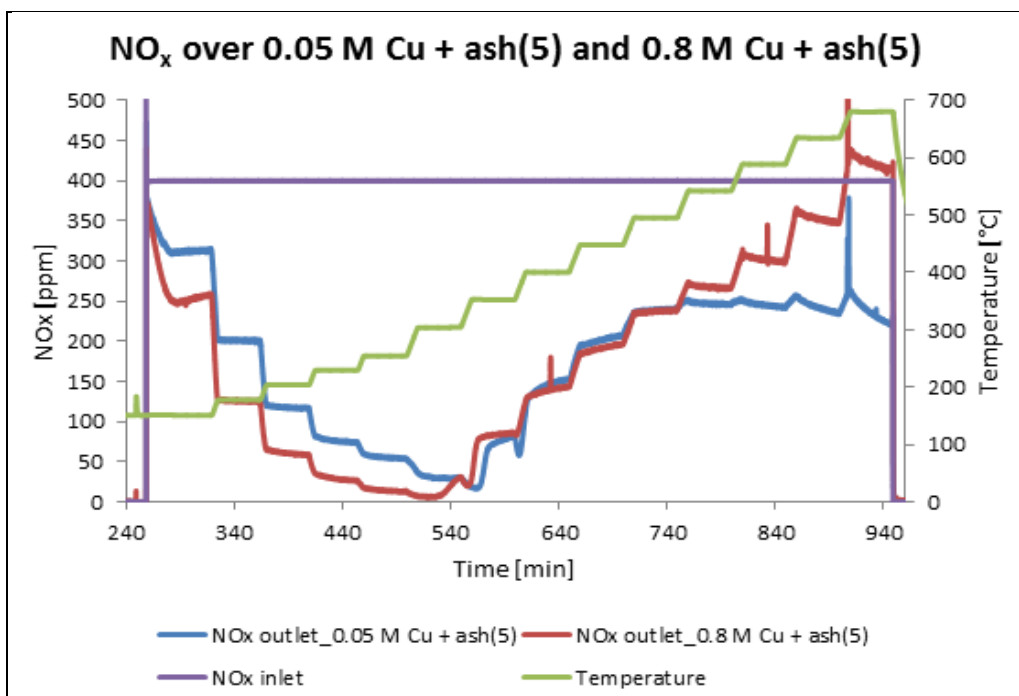

Figure 4.4-2: NO_x reduction activity comparison between 0.05 M Cu/SAPO-34 with 5 g/L ash and 0.8 M Cu/SAPO-34 with 5 g/L ash.

In fact, the ash "contamination" decreases the NO_x conversion, only at high temperatures, yet for both highly and lowly Cu-loaded samples. The Cu-based catalysts coated with ash exhibit high NH_3 oxidation to NO, resulting in poor NO_x conversion during NH_3-SCR.

### 4.4.1. *Production of N_2O and CO_2 over Samples with Ash (5 g/L)*

The decrease in NO_x conversion in relation to the formation of N_2O indicates again the oxidation of NH_3 at high temperatures. As previously stated, at temperatures ≥300°C the formation of undesired by-product N_2O reveals that NH_3 has been partially oxidised by O_2 [58].
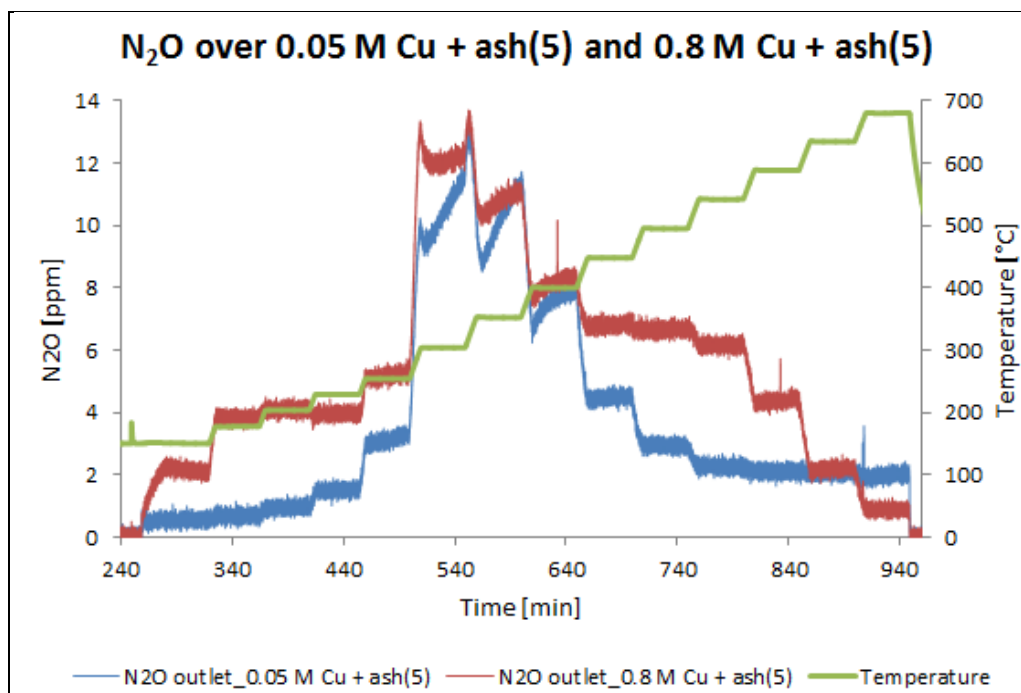
Figure 4.4-3: N$_2$O concentration comparison between 0.05 M Cu/SAPO-34 with 5 g/L ash and 0.8 M Cu/SAPO-34 with 5 g/L ash.

As seen in **Fig. 4.4-3.**, both Cu loading and ash coverage on the SCR catalysts result in increased formation of N$_2$O up to 12 ppm. Hence, there is a relatively large formation of N$_2$O herein, since the Cu/SAPO-34 coated with ash is more selective toward N$_2$O than the fresh Cu/SAPO-34 (see **Fig. 4.3-3.**). This is mainly apparent in the intermediate temperatures of 300-350°C, in direct contrast to the previous case of catalysts without ash.
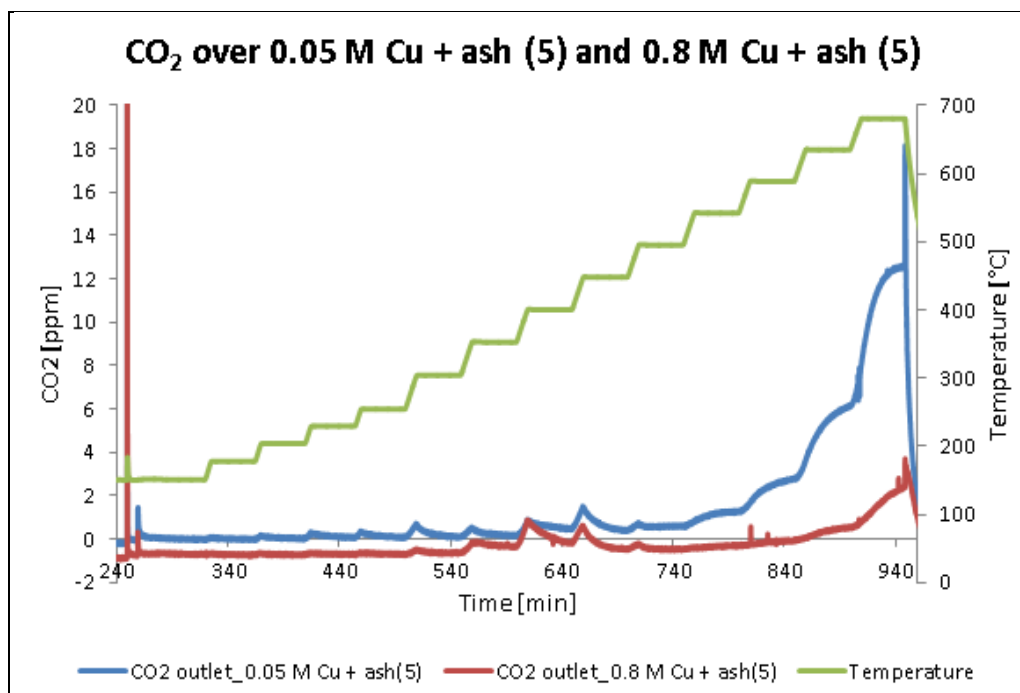
Figure 4.4-4: CO_2 concentration comparison between 0.05 M Cu/SAPO-34 with 5 g/L ash and 0.8 M Cu/SAPO-34 with 5 g/L ash.

The relative concentration of CO_2 is shown in **Fig. 4.4-4.** for the samples coated with ash of 5 g/L. Even though CO_2 production is generally insubstantial, at temperatures higher than 500°C the CO_2 concentration seems to increase reaching 12 ppm for the ash-coated Cu/SAPO-34 with 0.05 M Cu content. This result leads to the conclusion that there might be some coke residues in the ash that is oxidised at high temperatures for 0.05 M Cu/SAPO-34, compared to 0.8 M Cu/SAPO-34 which exhibits negligible CO_2 formation.

4.5. Micro-calorimeter Study I – NH_3 Oxidation

To understand the decline in NO_x reduction activity at higher temperatures during the SCR process, an experiment for the oxidation of NH_3 is performed in the micro-calorimeter instrument over the ash powder sample. This sample is exposed to treatment of 500 ppm NH_3 and 8% O_2 at 50°C for 3 h. Then the temperature is ramped up to 700°C with a ramping rate of 5°C min^{-1} in the same gas mixture (NH_3, O_2 and balanced Ar) and the results are found in **Fig. 4.5.** below.
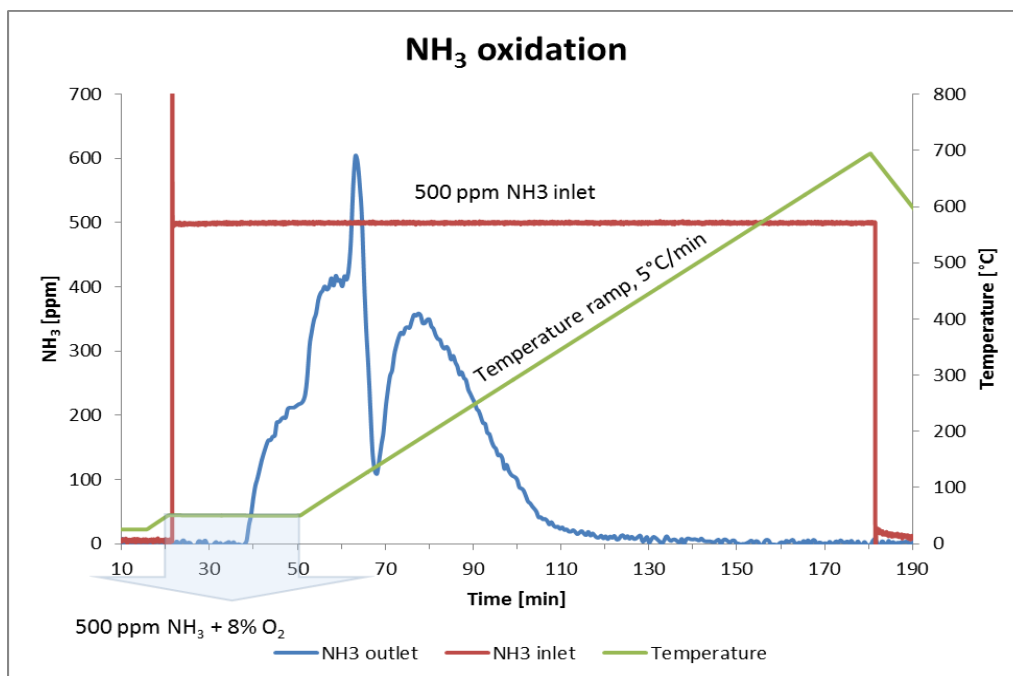
Figure 4.5: Micro-calorimeter experiment over 100 mg ash sample for NH$_3$ oxidation reaction.

The results in **Fig. 4.5.** further validate the findings about NH$_3$ oxidation at high temperatures by showing the oxidation abilities over ash. Ammonia is initially stored on the ash, resulting in a total uptake of ammonia, which will be further discussed in a subsequent chapter (see **4.9.**). When increasing the temperature, an ammonia desorption is visible. At higher temperatures, all ammonia is consumed, which clearly indicates a large ammonia oxidation over ash above 350°C. These calorimetric results on NH$_3$ oxidation over ash are in agreement with the increased NH$_3$ oxidation reaction during NH$_3$-SCR at high temperatures in the presence of ash, resulting in decreased NO$_x$ conversion over the Cu/SAPO-34 catalysts deposited with ash (**Fig. 4.4-2.**).

4.6. ICP-SFMS Measurements on Ash Composition

According to the *Inductively Coupled Plasma-Sector Field Mass Spectrometry* (ICP-SFMS) analysis of the ash powder conducted by ALS Scandinavia AB and used in this work, the composition of ash is summarized in the following **Table 2**, where TS is the dry weight and LOI stands for "Lost On Ignition".

As can be seen, the ash sample contains significant amounts of Fe$_2$O$_3$ (25.6%), CaO (7.69%), SiO$_2$ (6.33%), P$_2$O$_5$ (5.58%), large amounts of nonmetal S (3.28%) and the heavy post-transition metal Zn (2.62%), as well as fairly big fractions of transition metals Cu (0.676%), Ni (0.389%) and Cr (0.267%). Small portions of other transition metals, such as Zr (490 mg/kg), Mo (296 mg/kg) and V (250 mg/kg), as well as the precious metals Pt (373 mg/kg), Pd (94 mg/kg) and Rh (1.63 mg/kg) are also detected herein. In the **Table 2**, some of the largest amounts measured in the ash powder are highlighted with red.

ELEMENT	Sample (mg/kg TS)
As	6.41
Ba	180
Be	0.694
Cd	0.774
Co	28.8
Cr	**2670**
Cu	**6760**
Hg	0.0181
Mo	296
Nb	47.4
Ni	**3890**
Pb	79.9
Pd	94
Pt	**373**
Rh	1.63
S	**32800**
Sb	5.4
Sc	1.18
Se	<1
Sn	99.1
Sr	140
V	250
W	<50
Y	11
Zn	**26200**
Zr	**490**

| ELEMENT	Sample (% TS)
TS	99.1
SiO_2	6.33
Al_2O_3	2.64
CaO	7.69
Fe_2O_3	**25.6**
K_2O	0.278
MgO	0.566
MnO	0.13
Na_2O	0.606
P_2O_5	5.58
TiO_2	0.101
Summa	49.5
LOI 1000°C	8.8

Sulphur (S) is found in the fuel and this is the reason for the large amounts of sulphur in the ash sample. In addition to sulphur, other elements such as phosphorus (P), zinc (Zn) and calcium (Ca) are often present in lubricant oils and therefore end up in the ash. It should be noted that the ash used in this work is originating from a company that renovates filters. Thus, in the renovating process it is likely that if the filter contained an active coating, then some part of the catalyst has fallen off and is present in the ash.

There are two common types of catalytic filters, which are the SCR coated filters as well as the oxidation filters. For the oxidation filters, precious metals are common and this is likely the reason that Pt, Pd and Rh are found in the ash. By contrast, in the SCR coated filters it could be copper or iron zeolites or vanadia-based systems. Indeed, copper and vanadia are found by this ICP-SFMS analysis of the ash powder. Another contribution to the ash is from engine wear, and the presence of Cu-Ni-Fe-Cr- fragments, as small as tens of nm within the ash, is ascribed to engine wear since the fragments probably come from abraded engine parts.

4.7. Study III – Effect of Ash Loading on 0.05 M Cu/SAPO-34

As for ash and its effect, characterization of catalysts containing different ash loadings (serving as coatings) is investigated using *"standard SCR"* activity experiments in the fixed-bed reactor. Nevertheless, no previous work has been reported on this subject except for a study about the feasibility of using fly ash as a catalyst support, not only as a coating [69].

The experimental results about the NH_3 and NO_x conversions for the catalyst with low Cu content and ash are shown in **Fig. 4.7-1.** and **Fig. 4.7-2.**, respectively. A stepwise temperature increase from 150 up to 700°C comprises the reaction temperature range. The gas mixture consists of 400 ppm NO, 400 ppm NH_3, 8% O_2 and 5% H_2O, balanced with Ar again.
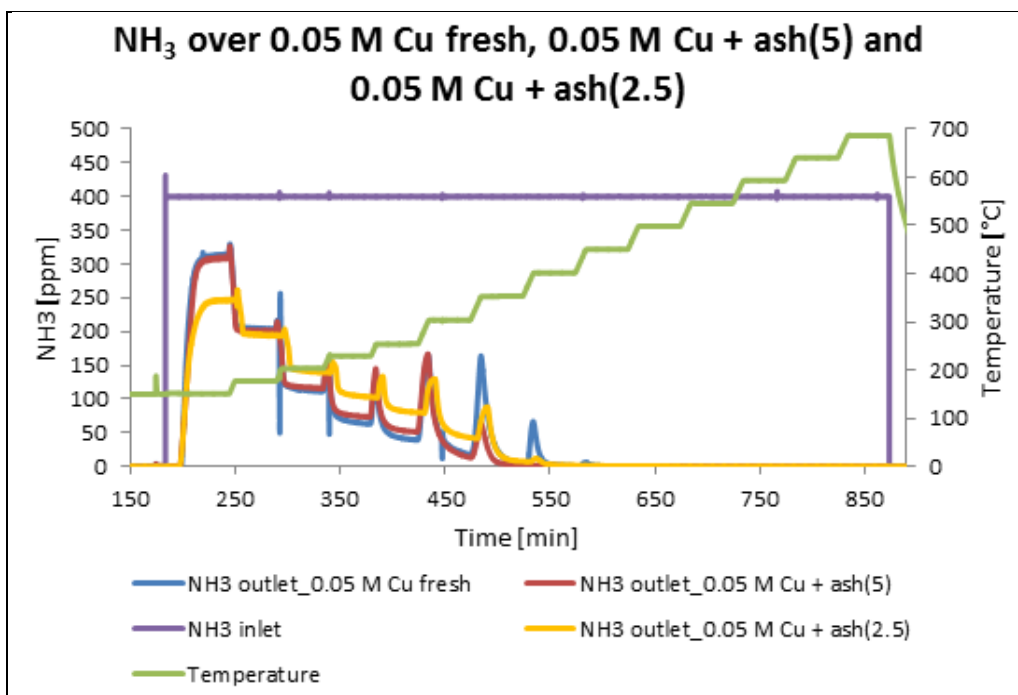
Figure 4.7-1: NH₃-SCR activity comparison among fresh 0.05 M Cu/SAPO-34, 0.05 M Cu/SAPO-34 with 5 g/L ash, and 0.05 M Cu/SAPO-34 with 2.5 g/L ash.

The fresh sample and the 5 g/L ash-loaded sample behave similarly at low temperatures, while lower NH_3 and NO_x concentrations are found at 150°C when 2.5 g/L ash is loaded (yellow curve in **Fig. 4.7-1.** and **Fig. 4.7-2.**). Hence, for the latter sample, the catalytic activity starts at concentrations lower than those for the fresh sample and the sample with 5 g/L ash. However, the reason for this observation is not clear. It is also obvious that the decrease in NO_x conversion starts at 300°C for samples with ash, while this decrease starts above 500°C for the fresh sample without ash (**Fig. 4.7-2.**).
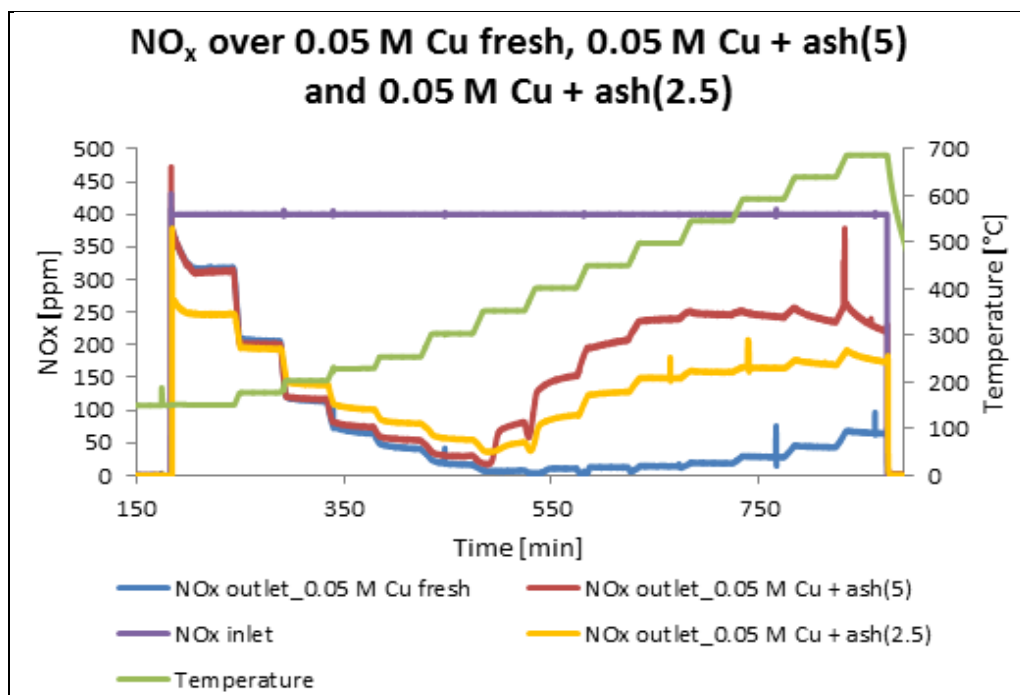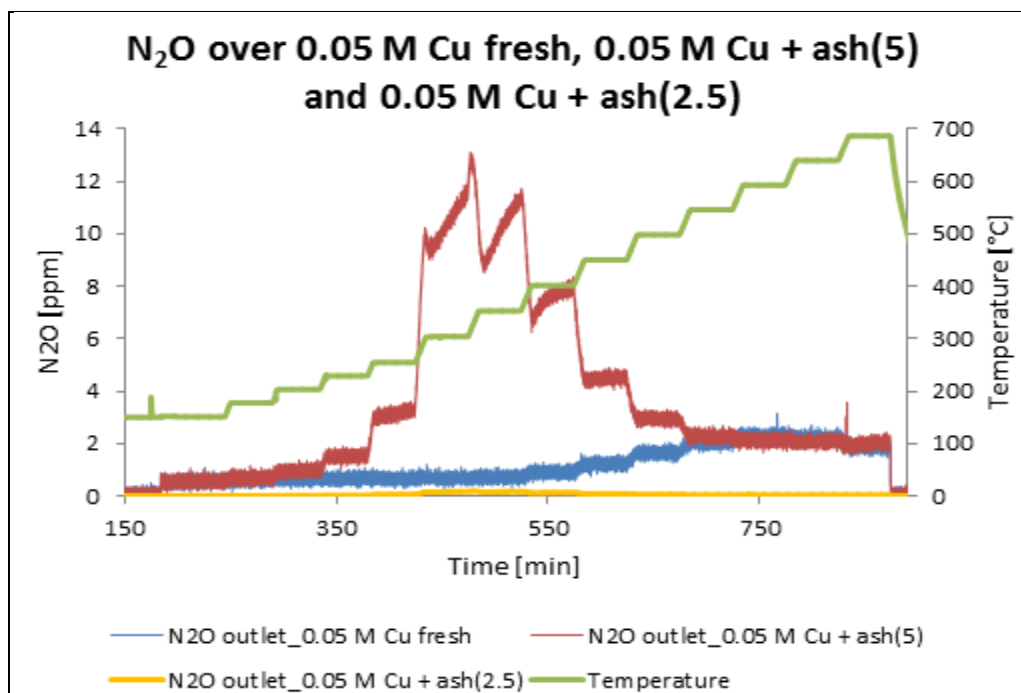
Figure 4.7-2: NO$_x$ reduction activity comparison among fresh 0.05 M Cu/SAPO-34, 0.05 M Cu/SAPO-34 with 5 g/L ash, and 0.05 M Cu/SAPO-34 with 2.5 g/L ash.

A maximum is approximated at around 550°C for the sample with ash of 5 g/L, while for the sample with half ash loading the outlet concentration of NO$_x$ is also half, as expected. At temperatures higher than the peak conversion temperature window, the NO$_x$ conversion rapidly decreases probably due to the increased ammonia oxidation to produce N$_2$.

Consequently, higher NO$_x$ conversion at high temperatures is observed for fresh Cu-based catalyst (**Fig. 4.7-2.**) compared to 2.5 g/L and 5 g/L ash-loaded samples, but ash significantly decreases the NO$_x$ conversion. The reason for this is likely due to increased NH$_3$ oxidation in the presence of precious metals in the ash, which favour the reaction. These precious metals are identified and confirmed for the ash sample by ICP-SFMS analysis (see **Table 2**). This leads to the conclusion that, although NO$_x$ reduction and NH$_3$ oxidation rates are mainly correlated to the amount of metal ions (i.e. metal content), ash coverage also plays a significant role in the whole process.

4.7.1 *Production of N$_2$O and CO$_2$ over 0.05 M Cu/SAPO-34 with Ash*

The **Fig. 4.7-3.** illustrates that a fairly large N$_2$O amount of 10-12 ppm is formed at 300-350°C for 0.05 M Cu/SAPO-34 sample loaded with 5 g/L ash, suggesting the effect of ash loading on the N$_2$O production. There is an almost negligible N$_2$O production for the fresh Cu/SAPO-34 catalyst with 0.05 M Cu content and for the catalyst loaded with 2.5 g/L ash. This probably is a result of ineffective ash application on the catalyst or coverage with an undesired amount of ash at the preparation phase.

Figure 4.7-3: N₂O concentration comparison among fresh 0.05 M Cu/SAPO-34, 0.05 M Cu/SAPO-34 with 5 g/L ash, and 0.05 M Cu/SAPO-34 with 2.5 g/L ash.

With regards to CO_2 formation over the tested samples during SCR, **Fig. 4.7-4.** shows that about 12 ppm CO_2 are formed at the highest temperature (650-700°C) over 0.05 M Cu/SAPO-34 loaded with 5 g/L ash (see also **Fig. 4.4-4.**). Even though CO_2 production is generally weak, this finding suggests that there are some coke residues in the ash and therefore an ash oxidation reaction occurs at temperatures higher than 500°C.
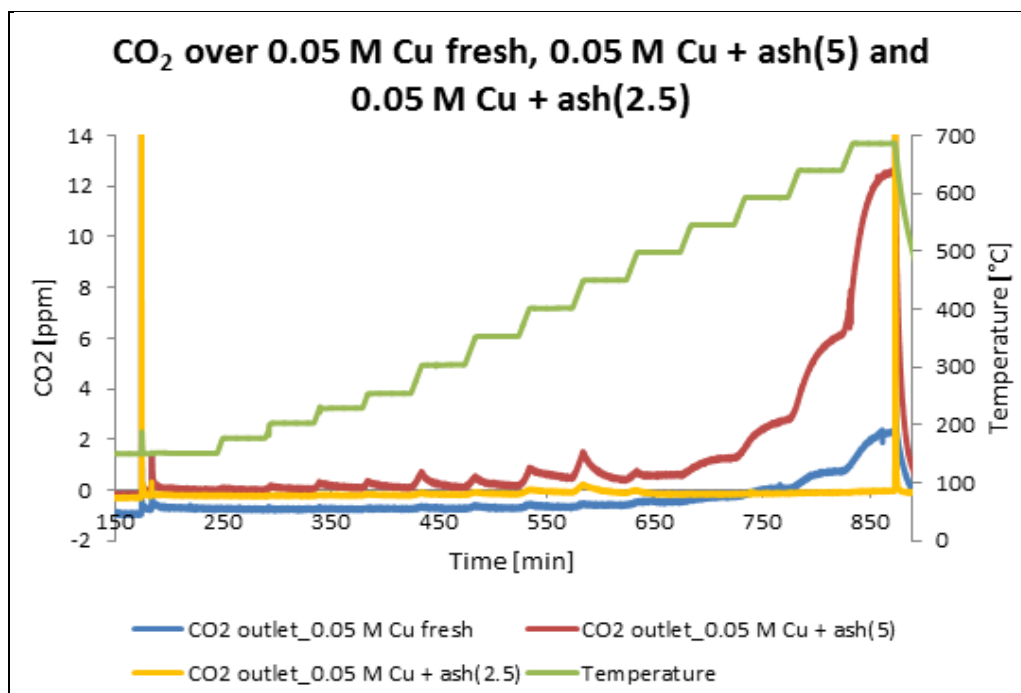
Figure 4.7-4: CO_2 concentration comparison among fresh 0.05 M Cu/SAPO-34, 0.05 M Cu/SAPO-34 with 5 g/L ash, and 0.05 M Cu/SAPO-34 with 2.5 g/L ash.

4.8. Study IV – Effect of Ash Loading on 0.8 M Cu/SAPO-34

The effect of ash on the NH_3-SCR activity and NO_x reduction ability for Cu/SAPO-34 catalyst with the high Cu content is shown in **Fig. 4.8-1.** and **Fig. 4.8-2.**, respectively. The reaction conditions are the same as the ones used for the 0.05 M Cu/SAPO-34 sample.

Higher NH_3 and NO_x conversions at 150^oC are observed for 2.5 g/L ash-loaded sample (yellow curve) compared to the other samples. This finding is similar to the result for the 0.05 M Cu/SAPO-34 catalyst loaded with 2.5 g/L ash and the reason for this needs further investigation.

Also, upon comparison, the decreasing trends of NO_x and NH_3 concentrations are similar for fresh sample and sample with 5 g/L ash at low temperatures (below 350^oC). Hence, the amount of ash powder on the catalyst has little next to negligible effect on both the NH_3-SCR and the deNO$_x$ activities below 350^oC (**Fig. 4.8-1.** and **Fig. 4.8-2.**).

However, the total NH_3 conversion starts at a lower temperature (>300°C) for the samples coated with ash in contrast to the fresh one without ash (>350°C). At high temperatures (above 350^oC) NH_3 is completely consumed and thus total conversion for NH_3 is revealed for all three samples (**Fig. 4.8-1.**).
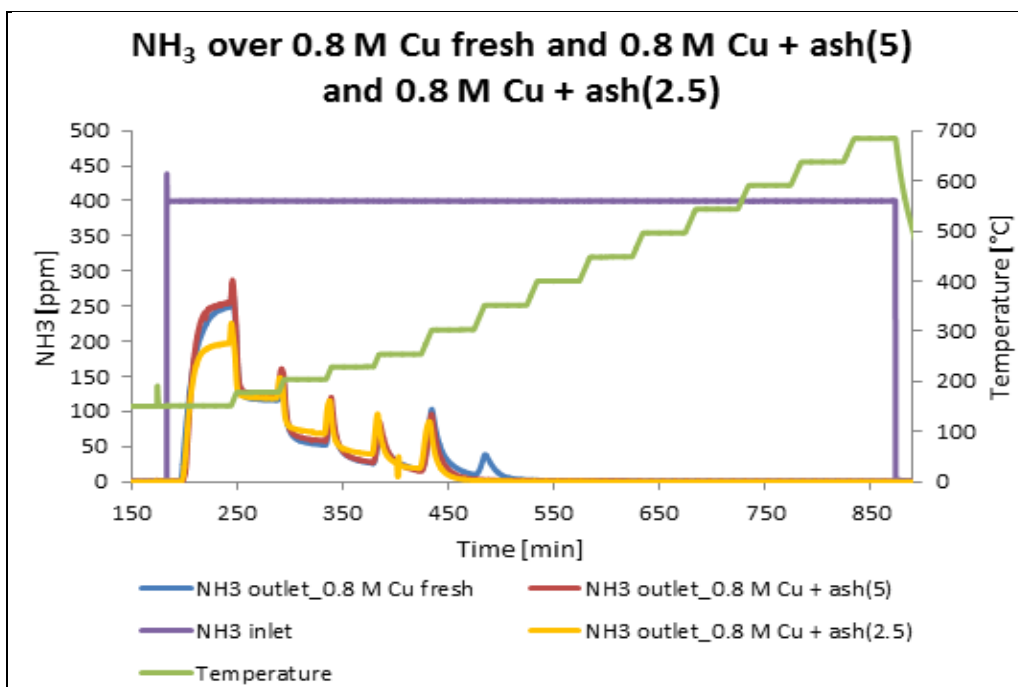
Figure 4.8-1: NH₃-SCR activity comparison among fresh 0.8 M Cu/SAPO-34, 0.8 M Cu/SAPO-34 with 5 g/L ash, and 0.8 M Cu/SAPO-34 with 2.5 g/L ash.

Similarly, it is clear that the decrease in NO_x conversion starts at 300°C for the samples with ash, while this decrease starts above 350°C for the fresh sample without ash (**Fig. 4.8-2.**).
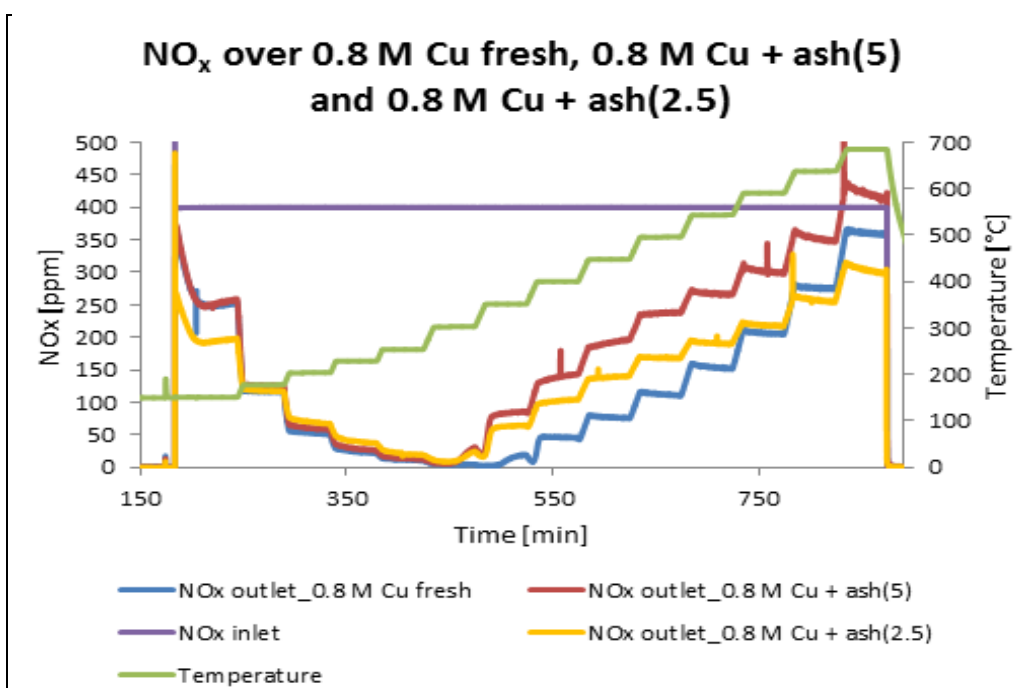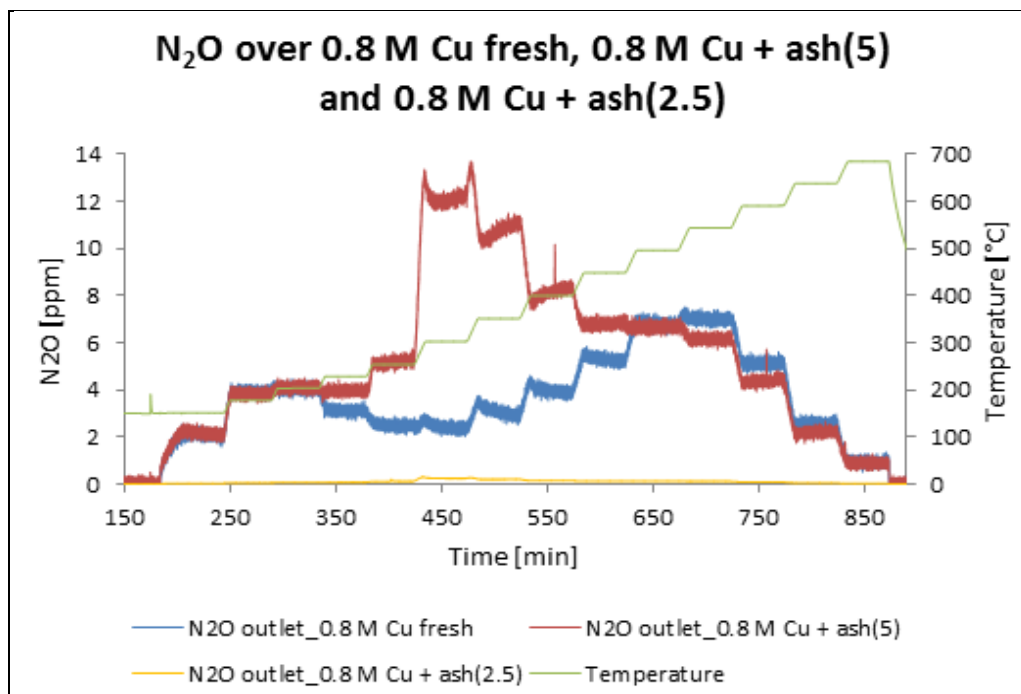

Figure 4.8-2: NO$_x$ reduction activity comparison among fresh 0.8 M Cu/SAPO-34, 0.8 M Cu/SAPO-34 with 5 g/L ash, and 0.8 M Cu/SAPO-34 with 2.5 g/L ash.

In addition, it can be suggested from **Fig. 4.8-2.** that the order of catalysts for their NO_x conversion at high temperatures (above 300°C) from the best to the poorest catalytic activity can be: fresh > 2.6Cu + 2.5g/L ash > 2.6Cu + 5g/L ash. For instance, the 0.8 M Cu/SAPO-34 sample with 5 g/L ash exhibits worse NO_x conversion with temperature than the other samples. Apparently, half ash loading with regards to the one originally used (i.e. ash of 17.5 mg instead of 35 mg) lowers the effect of ash to about half at high temperatures.

Hence, the results show that the parameters "ash coverage" and "temperature" strongly affect the catalytic activity. The increasing temperatures quickly reduce the NO_x conversion rate and slow the catalytic activity. Also, the higher the ash content the poorer the NO_x conversion, meaning the more ash there is over the catalyst sample the worse the NO_x conversion becomes due to NH_3 oxidation during NH_3-SCR. The reason for this, as discussed above, is the presence of small amounts of precious metals in the ash that increases the ammonia oxidation.

4.8.1. *Production of N_2O and CO_2 over 0.8 M Cu/SAPO-34 with Ash*

The catalytic performances of the fresh sample and ash-loaded Cu/SAPO-34 samples, with high Cu content in both cases, are compared in terms of N_2O and CO_2 production during NH_3-SCR. It is found that a higher N_2O concentration of 12 ppm exists at 300°C for 0.8 M Cu/SAPO-34 sample with 5 g/L ash (**Fig. 4.8-3.**), suggesting that high ash loading influences the N_2O formation (compared to the fresh sample and the sample with 2.5 g/L ash). This might be due to the platinum residues in the ash, since Pt is a catalyst that is known to oxidise ammonia effectively with very high selectivity to N_2O.

Figure 4.8-3: N_2O concentration comparison among fresh 0.8 M Cu/SAPO-34, 0.8 M Cu/SAPO-34 with 5 g/L ash, and 0.8 M Cu/SAPO-34 with 2.5 g/L ash.
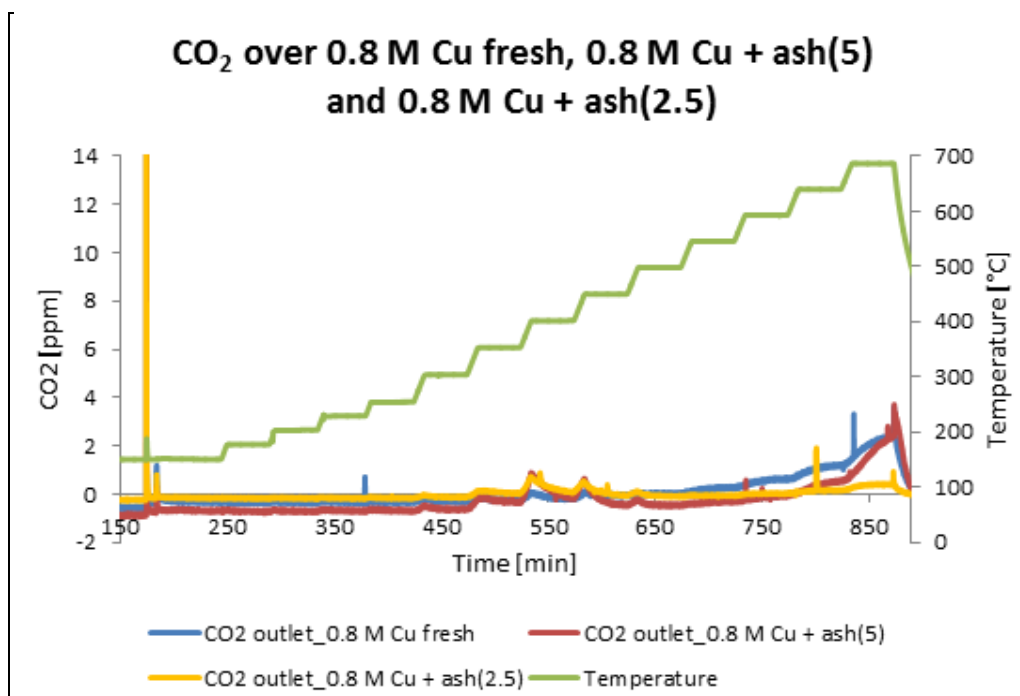
Figure 4.8-4: CO₂ concentration comparison among fresh 0.8 M Cu/SAPO-34, 0.8 M Cu/SAPO-34 with 5 g/L ash, and 0.8 M Cu/SAPO-34 with 2.5 g/L ash.

Regarding CO_2 formation over the highly Cu-loaded sample (**Fig. 4.8-4.**), negligible CO_2 amounts up to 1-2 ppm are formed at 700°C for the 0.8 M Cu-loaded sample with 5 g/L ash. Thus, no traces of coke are present in this sample compared to the previous case of 0.05 M Cu/SAPO-34 (**Fig. 4.7-4.**), where an ash oxidation reaction may occur above 500°C.

4.9. Micro-calorimeter Studies II – TPDs

Since the $deNO_x$ activity of NH_3-SCR catalysts is directly determined by the reactivity of NH_3 adsorbed onto the catalyst surface, all the adsorption and desorption phenomena of NH_3 are of utmost importance for this study. Ammonia storage capacity of the ash plays a significant role in the SCR system on the whole.

In this respect, the findings of the NH_3-TPD experiment concerning the inlet and outlet NH_3 concentrations are shown in **Fig. 4.9-1.**. During the adsorption period, the sample is exposed to 200 ppm NH_3 at 50°C for 2 h, followed by desorption period. So, after flushing with Ar for 30 min, the temperature is raised to 800°C with a ramping rate of 10°C min^{-1}.
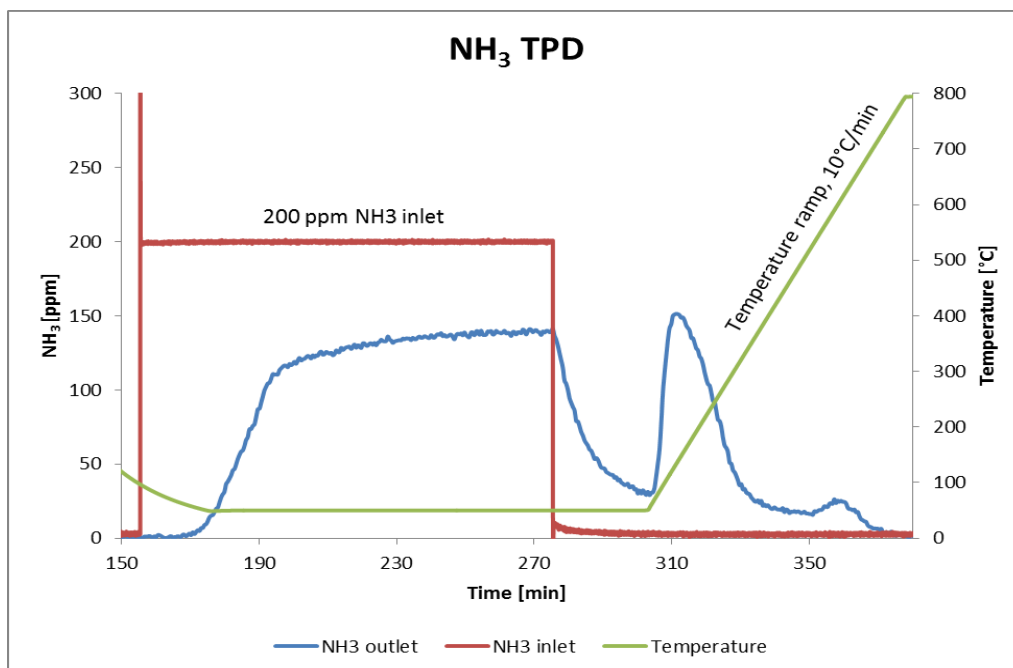
Figure 4.9-1: Micro-calorimeter experiment over 100 mg ash sample for NH$_3$ TPD.

During the exposure of the sample to NH$_3$, an almost complete NH$_3$ uptake is observed, followed by a breakthrough of NH$_3$ on the catalyst surface. Therefore, after the adsorption period, the ash powder is exposed to Ar alone and *loosely bound ammonia* is released. The temperature is then ramped up with 10°C min^{-1} rate to 800°C, and one desorption peak of *strongly bound ammonia* is produced (**Fig. 4.9-1.**).
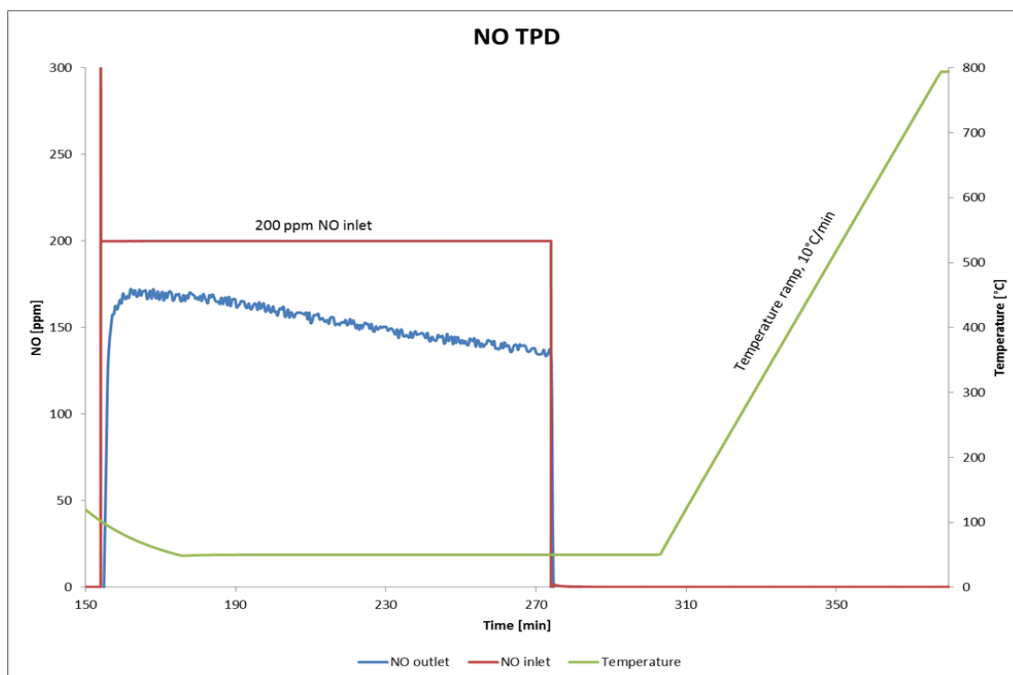
Figure 4.9-2: Micro-calorimeter experiment over 100 mg ash sample for NO TPD.

When using NO as adsorbate gas, the adsorption is carried out at 50°C and the sample is exposed to 200 ppm NO at 50°C for 2 h. Then, after flushing with Ar for 30 min, the temperature is increased to 800°C with 10°C min^{-1} ramping rate in Ar alone. The results are presented in **Fig. 4.9-2.** illustrating that NO is not adsorbed on the ash-loaded catalyst, which is also seen by the fact that no desorption peak is observed during the temperature ramping.
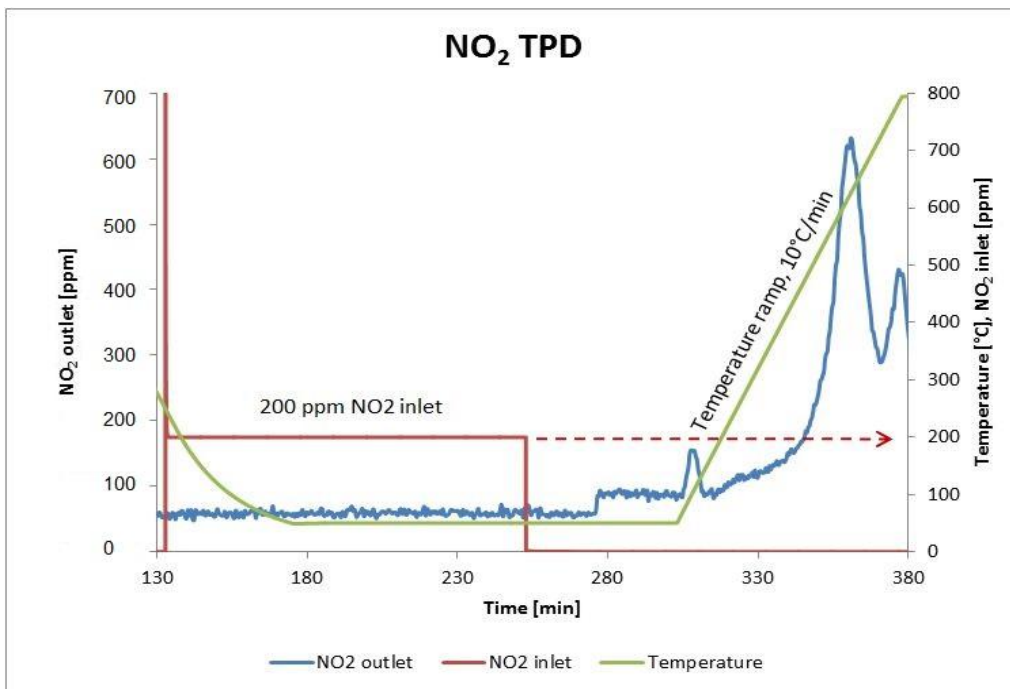
Figure 4.9-3: Micro-calorimeter experiment over 100 mg ash sample for NO$_2$ TPD.

The adsorption-desorption behavior of NO$_2$ during the NO$_2$ TPD experiment is also investigated through this work. The profiles of NO$_2$ and NO signals during the NO$_2$ TPD experiment are presented in **Fig. 4.9-3.** and **Fig. 4.9-4.**, respectively. The experimental results show that large amounts of NO$_2$ are stored in the ash sample. Therefore, NO and NO$_2$ desorption peaks are revealed during desorption period with a temperature ramping rate of 10°C min^{-1} up to 800°C.
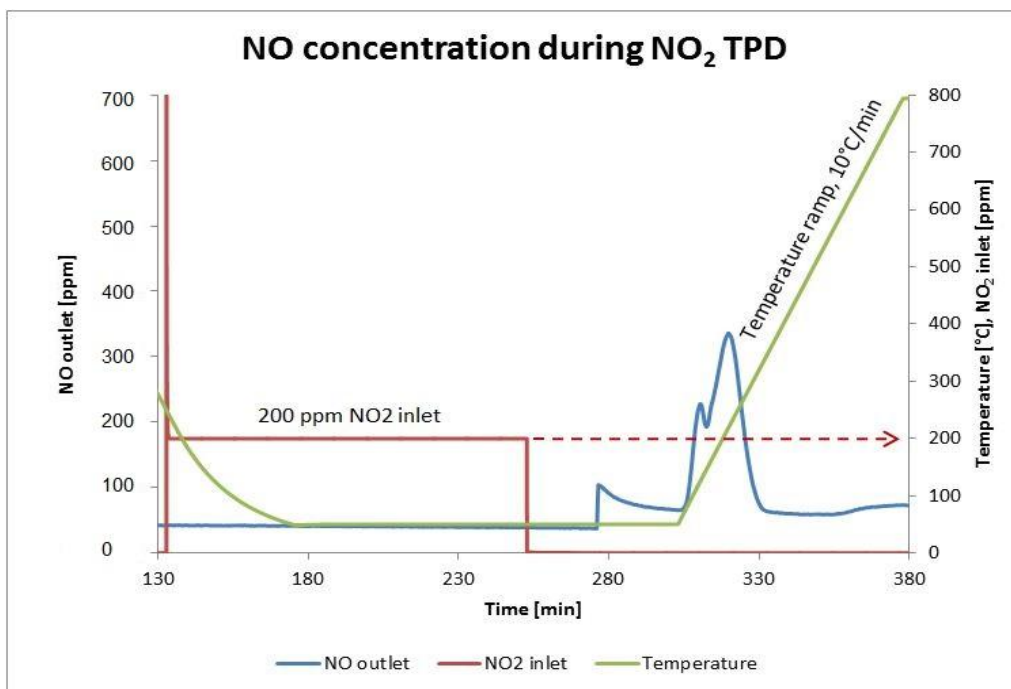
Figure 4.9-4: Micro-calorimeter experiment over 100 mg ash sample, depicting the NO signal during NO₂ TPD.

5. CONCLUSIONS

The first part of this thesis was the synthesis and aging of SAPO-34 zeolite, the wet ion exchange of two Cu contents (0.05 M and 0.8 M) into the SAPO-34 zeolite catalysts, the monoliths preparation and catalyst washcoating and, lastly, the deposition of certain ash amounts (2.5 and 5 g/L) on Cu/SAPO-34 catalyst-washcoated monoliths.

Our ash sample originated from renovated filters and was provided by Volvo Cars.

The second part was focused on the sample characterization. The fresh Cu-SAPO-34 catalysts were characterized with XRD technique and the XRD patterns confirmed the maintenance of the CHA structure in SAPO-34 zeolite after ion exchange synthesis. The composition of the ash was analyzed by ICP-SFMS.

The third part was directed on the flow reactor experiments for NH_3-SCR at a temperature range between 150 and 700^oC, and micro-calorimeter experiments.

Study I – The effect of Cu loading on fresh samples: The 0.8 M Cu-loaded sample exhibited outstanding NO_x and NH_3 conversion activities at low temperatures (150-300^oC). However, it possessed larger NH_3 oxidation and thus remarkably lower NO_x reduction activity at high temperatures (>350^oC) compared to the 0.05 M Cu-loaded sample. Also, a total NH_3 conversion at high temperatures (>400^oC) was presented for both fresh samples. This behavior was interpreted as an indication of the role of Cu species in the formation of active sites in SAPO-34 framework. High ion exchange level (i.e. high Cu content) was reported as being the condition for active site formation for ammonia oxidation reaction.

Study II – Effect of Cu loading on samples with ash (5 g/L): The samples coated with ash and the fresh samples exhibited similar trends, but different absolute concentrations. At high temperatures (>300^oC), for ash-loaded samples a decrease in NO_x conversion appeared on both high and low Cu-containing samples in contrast to fresh samples. So, both possessed high NH_3 oxidation, leading to worse NO_x conversions.

Micro-calorimeter study I – NH_3 oxidation: This result validated the findings about high NH_3 oxidation at high temperatures by illustrating the oxidation abilities over ash. Initially, NH_3 was stored on the ash, seen by a total uptake of NH_3, whereas with increasing temperature an NH_3 desorption appeared, and finally all ammonia was consumed, due to NH_3 oxidation over ash above 350^oC.

ICP-SFMS measurements on ash composition: The ash powder sample was found to contain considerable amounts of Fe_2O_3, CaO, SiO_2 and P_2O_5, large amounts of S, as well as the transition metals Zn, Cu, Ni, Cr, Zr, Mo and V. The precious metals Pt, Pd and Rh were also detected by ICP-SFMS analysis. Sulphur, phosphorus, zinc and calcium ended up in the ash, because they are present in lubricant oils. Also, precious metals are commonly found in oxidation filters, while Cu- or Fe- zeolites or V-based systems could be in SCR coated filters, and Cu-Ni-Fe-Cr- fragments might come from wear of engine parts.

Study III – Effect of ash loading on 0.05 M Cu/SAPO-34: The fresh sample and the 5 g/L ash-loaded sample exhibited similar behaviour at low temperatures, whereas when 2.5 g/L ash were deposited, lower NH_3 and NO_x concentrations were measured at $150^{\circ}C$. However, the reason for this observation was unclear. At high temperatures, the fresh 0.05 M Cu-based catalyst possessed higher NO_x conversion compared to 2.5 and 5 g/L ash-loaded samples, and ash considerably decreased the NO_x conversion due to increased NH_3 oxidation to N_2. This phenomenon was likely due to the presence of precious metals in the ash, as confirmed by the ICP-SFMS analysis.

Study IV – Effect of ash loading on 0.8 M Cu/SAPO-34: As previously, the 2.5 g/L ash-loaded sample exhibited higher NH_3 and NO_x conversions at $150^{\circ}C$, compared to the other samples, and the reason for this needs further investigation. Apart from this, the behaviour of NH_3 and NO_x concentrations was similar for all samples at low temperatures ($<350^{\circ}C$), and therefore the amount of ash had negligible effect on catalytic activity. Above $350^{\circ}C$, the ammonia was completely consumed and thus a total conversion of NH_3 was revealed for all samples.

For high Cu-loaded samples, the following order of samples for their NO_x conversion at high temperatures was suggested (from the best to the worst catalytic activity): fresh 0.8Cu > 0.8Cu + 2.5g/L ash > 0.8Cu + 5g/L ash. A respective trend was valid for the 0.05 M Cu-loaded samples as well. Consequently, the more ash there was over the catalyst sample, the poorer the NO_x conversion was, owing to NH_3 oxidation in the presence of small amounts of precious metals in the ash.

Micro-calorimeter studies II – TPDs: The ammonia storage capacity of 100 mg ash sample was examined through TPD experiments. At first, the result from NH_3 TPD showed that after the adsorption period, the ash powder was exposed to gas and *loosely bound ammonia* was released. When the temperature started being ramped up to $800^{\circ}C$, one desorption peak of *strongly bound ammonia* was formed. Secondly, the NO TPD revealed that NO was not adsorbed on the ash-loaded catalyst, seen also by that no desorption peak was produced during the temperature ramping. Thirdly, the NO_2 TPD results showed that large amounts of NO_2 were stored in the ash sample, and hence NO and NO_2 desorption peaks were observed during desorption period up to $800^{\circ}C$.

Production of N_2O: Over the fresh 0.8 M Cu-loaded sample, there appeared a first maximum of just 4 ppm N_2O around $200^{\circ}C$, because at low temperatures NH_3-NO species formation probably gave N_2O as a by-product during decomposition, and a second maximum of about 7 ppm at $550^{\circ}C$, since unwanted oxidising properties of the NH_3-SCR catalyst may have emerged. Blocking various zeolite cavities by using co-cations could alleviate this problem. Over the samples with 5 g/L ash, increased formation of N_2O up to 12 ppm was observed in the intermediate temperatures of $300-350^{\circ}C$, because these samples were more selective to N_2O than the fresh Cu/SAPO-34 samples.

In particular, over the 0.05 M Cu-loaded sample with 5 g/L ash, a fairly large amount of N_2O up to 10-12 ppm at $300-350^{\circ}C$ was produced in comparison to an almost negligible N_2O production for the fresh sample and the sample with 2.5 g/L ash. This was likely due to ineffective ash application on the catalyst or coverage with an undesirable ash amount for the 2.5 g/L sample.

By contrast, for the 0.8 M Cu-loaded sample with 5 g/L ash, the formation of 12 ppm N_2O at $300^{\circ}C$ suggested that a higher ash loading induced the N_2O production. This might have been due to the Pt residues in the ash, since Pt effectively oxidises NH_3 with very high selectivity to N_2O.

Production of CO_2: Even if CO_2 formation was insubstantial in general, CO_2 amounts reached about 12 ppm over the 0.05 M Cu-loaded sample with 5 g/L ash at the highest temperature $(650-700^{\circ}C)$. This observation was justified by some coke residues in the ash that was oxidised at temperatures above $500^{\circ}C$, and thus a coke oxidation reaction might have happened. On the contrary, negligible CO_2 amounts up to 2 ppm were produced over the 0.8 M Cu-loaded sample with 5 g/L ash at $700^{\circ}C$. Hence, no coke traces were presumed in this sample compared to the previous case of catalyst with low Cu content.

Future Outlook:

The successful treatment of engine exhaust gas using Cu zeolite catalysts has been already reported. Interesting things to further study is understanding of the local Cu structure and the role of preparation conditions. The main structural parameters controlling activity of the Cu zeolite catalysts are pore dimension and arrangement, ion exchange level, i.e. Cu/Al values, and Si/Al ratio.

A potential future study could be based on what was previously mentioned about the ash composition, adding that the catalytically active elements of the ash samples include Fe, Cu, Ni and even V. Catalysts with different active elements have different catalytic effects. It would therefore be interesting to further study the impact of ash that is not contaminated with material from the DPF coating.

6. ACKNOWLEDGEMENTS

This master thesis has been conducted for the fulfillment of the Master of Science degree in Applied Physics at Chalmers University of Technology, Göteborg. It has been performed within the Competence Centre for Catalysis and the Department of Chemistry and Chemical Engineering, Division of Chemical Engineering from January 20th 2015 to September 2015.

The thesis has been executed under the supervision of Dr. Oana Mihai (Post-doctoral researcher at the Division of Chemical Engineering) and Dr. Louise Olsson (Professor at the Division of Chemical Engineering).

I would like to express my gratitude to both Oana and Louise for their constant guidance, help and support. This thesis would not have been materialized without their precious input, as well as theoretical and technical insights.

I would like to thank my companions, during the course of my research, Maria Naharro, Fredrik Edman, Kristian Målbakken, Emma Persson, Sébastien Pissot, Fathyah Hanum Pamungkaningtyas, Ashri Nugrahini, Axel Olsson and Fredrik Billskog.

I would also like to extent my gratitude towards the researchers in the laboratories Kurnia Wijayanti and Dr. Kirsten Leistner (Post-doctoral researcher at the Division of Chemical Engineering) for providing invaluable solutions to some of the practical problems encountered during the experiments.

Finally, I would like to thank my family and friends that have stood by me through the entire period of my master thesis and have made this experience a memorable one in years to come. Without their great contribution I would not have been able to succeed in my goals so far.

Göteborg, September 2015
Anastasia Theotoki

7. REFERENCES

1. Deka, U., et al., *Local Environment and Nature of Cu Active Sites in Zeolite-Based Catalysts for the Selective Catalytic Reduction of NOx.* Acs Catalysis, 2013. **3**(3): p. 413-427.
2. Sappok, A. and V. Wong, *Ash effects on diesel particulate filter pressure drop sensitivity to soot and implications for regeneration frequency and DPF control.* SAE International Journal of Fuels and Lubricants, 2010. **3**(1): p. 380-396.
3. Vaaraslahti, K., et al., *Effect of lubricant on the formation of heavy-duty diesel exhaust nanoparticles.* Environmental Science and Technology, 2005. **39**(21): p. 8497-8504.
4. Riguetto, B.A., et al., *Surface Behavior of Alumina-Supported Pt Catalysts Modified with Cerium as Revealed by X-ray Diffraction, X-ray Photoelectron Spectroscopy, and Fourier Transform Infrared Spectroscopy of CO Adsorption.* The Journal of Physical Chemistry B, 2004. **108**(17): p. 5349-5358.
5. Holmgren, A., B. Andersson, and D. Duprez, *Interactions of CO with Pt/ceria catalysts.* Applied Catalysis B: Environmental, 1999. **22**(3): p. 215-230.
6. *Nitrogen Oxide (NOx) Pollution.* 2015, Icopal-Noxite UK. Available at: http://www.icopal-noxite.co.uk/nox-problem/nox-pollution.aspx.
7. Guan, B., et al., *Review of state of the art technologies of selective catalytic reduction of NOx from diesel engine exhaust.* Applied Thermal Engineering, 2014. **66**(1–2): p. 395-414.
8. Johnson, T.V., *Review of Vehicular Emissions Trends.* SAE Int. J. Engines, 2015. **8**(3).
9. Li, J., et al., *Low-temperature selective catalytic reduction of NOx with NH3 over metal oxide and zeolite catalysts—A review.* Catalysis Today, 2011. **175**(1): p. 147-156.
10. Tang, W., et al., *On-engine investigation of SCR on filters (SCRoF) for HDD passive applications.* SAE International Journal of Engines, 2013. **6**(2): p. 862-872.
11. Lee, J.H., M.J. Paratore, and D.B. Brown, *Evaluation of Cu-based SCR/DPF technology for diesel exhaust emission control.* SAE International Journal of Fuels and Lubricants, 2009. **1**(1): p. 96-101.
12. Ngan, E., et al., *Final tier 4 emission solution using an aftertreatment system with a fuel reformer, LNT, DPF and optional SCR.* SAE Technical Papers, 2011.
13. Ogyu, K., et al., *Development of high porosity SiC-DPF which is compatible with high robustness and catalyst coating capability for SCR coated DPF application.* SAE Technical Papers, 2013. **2**.
14. Twigg, M.V., *Progress and future challenges in controlling automotive exhaust gas emissions.* Applied Catalysis B: Environmental, 2007. **70**(1-4): p. 2-15.
15. Liati, A., et al., *Investigation of diesel ash particulate matter: A scanning electron microscope and transmission electron microscope study.* Atmospheric Environment, 2012. **49**: p. 391-402.
16. Liati, A., et al., *Microscopic investigation of soot and ash particulate matter derived from biofuel and diesel: implications for the reactivity of soot.* Journal of Nanoparticle Research, 2012. **14**(11): p. 1-18.
17. Coda Zabetta, E., M. Hupa, and S. Niemi, *Bio-derived fuels may ease the regeneration of diesel particulate traps.* Fuel, 2006. **85**(17-18): p. 2666-2670.
18. Liati, A., et al., *Comparative studies of particles deposited in diesel particulate filters operating with biofuel, diesel fuel and fuel blends.* SAE Technical Papers, 2011.
19. Sappok, A., et al., *Theoretical and Experimental Analysis of Ash Accumulation and Mobility in Ceramic Exhaust Particulate Filters and Potential for Improved Ash Management.* SAE International Journal of Fuels and Lubricants, 2014. **7**(2): p. 511-524.
20. Majewski, W.A., *Soot Load Determination. 4.2 Design and Optimization. Diesel Filter Systems.* 2015, DieselNet Technology Guide. Available at: https://www.dieselnet.com/tech/dpf_sys.php#activ.
21. Kim, K., et al., *An investigative study of sudden pressure increase phenomenon across the DPF.* SAE Technical Papers, 2014. **1**.
22. Hohl, Y., *"SCR on Filter - The Future for Construction Machinery"*, in *10th International CTI Conference, SCR Systems.* 2014, July 8: Stuttgart.
23. Lee, K., Choi, S., Seong, H., *"Particulate Emissions Control by Advanced Filtration Systems for GDI Engines"*, in *DoE Annual Merit Review Meeting.* 2014, June 19: Washington DC.
24. Maunula, T., *Intensification of catalytic aftertreatments systems for mobile applications.* SAE Technical Papers, 2013. **2**.

25. Fang, H.L. and H.F.M. DaCosta, *Urea thermolysis and NOx reduction with and without SCR catalysts.* Applied Catalysis B: Environmental, 2003. **46**(1): p. 17-34.

26. Brandenberger, S., et al., *The State of the Art in Selective Catalytic Reduction of NOx by Ammonia Using Metal- Exchanged Zeolite Catalysts.* Catalysis Reviews-science and Engineering, 2008. **50**(4): p. 492-531.

27. Madia, G., et al., *Side reactions in the selective catalytic reduction of NOx with various NO2 fractions.* Industrial and Engineering Chemistry Research, 2002. **41**(16): p. 4008-4015.

28. Yun, B.K. and M.Y. Kim, *Modeling the selective catalytic reduction of NOx by ammonia over a Vanadia-based catalyst from heavy duty diesel exhaust gases.* Applied Thermal Engineering, 2013. **50**(1): p. 152-158.

29. Madia, G., et al., *Thermal stability of vanadia-tungsta-titania catalysts in the SCR process.* Applied Catalysis B: Environmental, 2002. **39**(2): p. 181-190.

30. Brandenberger, S., et al., *Estimation of the fractions of different nuclear iron species in uniformly metal-exchanged Fe-ZSM-5 samples based on a Poisson distribution.* Applied Catalysis A: General, 2010. **373**(1–2): p. 168-175.

31. Deka, U., et al., *Confirmation of isolated Cu 2+ ions in SSZ-13 zeolite as active sites in NH 3-selective catalytic reduction.* Journal of Physical Chemistry C, 2012. **116**(7): p. 4809-4818.

32. Fickel, D.W., et al., *The ammonia selective catalytic reduction activity of copper-exchanged small-pore zeolites.* Applied Catalysis B: Environmental, 2011. **102**(3-4): p. 441-448.

33. Berggrund, M., et al., *Influence of Synthesis Conditions for ZSM-5 on the Hydrothermal Stability of Cu-ZSM-5.* Catalysis Letters, 2009. **130**(1-2): p. 79-85.

34. *Zeolite Catalysis: Principles and Applications,Subhash Bhatia,CRC Press,Inc.,Boca Raton,USA,1990,ISBN 0-8493-5628-8,pp.291.* Applied Catalysis, 1991. **70**(1): p. N12-N14.

35. Baerlocher, C. and L. McCusker, *Commission of the International Zeolite Association (IZA-SC).* 2015, Database of Zeolite Structures. Available at: http://www.iza-structure.org/databases/Structure.

36. Vennestrøm, P.N.R., et al., *Migration of Cu ions in SAPO-34 and its impact on selective catalytic reduction of NOx with NH3.* ACS Catalysis, 2013. **3**(9): p. 2158-2161.

37. Wang, J., et al., *The influence of silicon on the catalytic properties of Cu/SAPO-34 for NOx reduction by ammonia-SCR.* Applied Catalysis B: Environmental, 2012. **127**(0): p. 137-147.

38. Wang, L., et al., *Location and nature of Cu species in Cu/SAPO-34 for selective catalytic reduction of NO with NH3.* Journal of Catalysis, 2012. **289**(0): p. 21-29.

39. Wang, L., et al., *Migration of Cu species in Cu/SAPO-34 during hydrothermal aging.* Journal of Catalysis, 2013. **306**(0): p. 68-77.

40. Xue, J., et al., *Characterization of copper species over Cu/SAPO-34 in selective catalytic reduction of NOx with ammonia: Relationships between active Cu sites and de-NOx performance at low temperature.* Journal of Catalysis, 2013. **297**(0): p. 56-64.

41. Kwak, J.H., et al., *Excellent activity and selectivity of Cu-SSZ-13 in the selective catalytic reduction of NOx with NH3.* Journal of Catalysis, 2010. **275**(2): p. 187-190.

42. Kwak, J.H., et al., *Effects of hydrothermal aging on NH3-SCR reaction over Cu/zeolites.* Journal of Catalysis, 2012. **287**(0): p. 203-209.

43. Ma, L., et al., *Characterization of commercial Cu-SSZ-13 and Cu-SAPO-34 catalysts with hydrothermal treatment for NH3-SCR of NOx in diesel exhaust.* Chemical Engineering Journal, 2013. **225**(0): p. 323-330.

44. Yang, X., et al., *Heterometal incorporation in metal-exchanged zeolites enables low-temperature catalytic activity of NO x reduction.* Journal of Physical Chemistry C, 2012. **116**(44): p. 23322-23331.

45. Colombo, M., I. Nova, and E. Tronconi, *A comparative study of the NH3-SCR reactions over a Cu-zeolite and a Fe-zeolite catalyst.* Catalysis Today, 2010. **151**(3–4): p. 223-230.

46. Schmieg, S.J. and J.H. Lee, *Evaluation of supplier catalyst formulations for the selective catalytic reduction of NOx with ammonia.* SAE Technical Papers, 2005.

47. Kamasamudram, K., et al., *Why Cu- and Fe-zeolite SCR catalysts behave differently at low temperatures.* SAE International Journal of Fuels and Lubricants, 2010. **3**(1): p. 664-672.

48. Pieterse, J.A.Z., S. Booneveld, and R.W. van den Brink, *Evaluation of Fe-zeolite catalysts prepared by different methods for the decomposition of N2O.* Applied Catalysis B: Environmental, 2004. **51**(4): p. 215-228.

49. Kumar, M.S., et al., *On the nature of different iron sites and their catalytic role in Fe-ZSM-5 DeNOx catalysts: new insights by a combined EPR and UV/VIS spectroscopic approach.* Journal of Catalysis, 2004. **227**(2): p. 384-397.

50. Chen, H.-Y. and W.M.H. Sachtler, *Activity and durability of Fe/ZSM-5 catalysts for lean burn NOx reduction in the presence of water vapor.* Catalysis Today, 1998. **42**(1–2): p. 73-83.

51. Feng, X. and W. Keith Hall, *FeZSM-5: A Durable SCR Catalyst for NOxRemoval from Combustion Streams.* Journal of Catalysis, 1997. **166**(2): p. 368-376.

52. Marturano, P., A. Kogelbauer, and R. Prins, *Preparation of Overexchanged Fe–ZSM-5 Zeolites Using the Ferrous Oxalate Method: Why Does It Fail?* Journal of Catalysis, 2000. **190**(2): p. 460-468.

53. Long, R.Q. and R.T. Yang, *Characterization of Fe-ZSM-5 catalyst for selective catalytic reduction of nitric oxide by ammonia.* Journal of Catalysis, 2000. **194**(1): p. 80-90.

54. Melián-Cabrera, I., et al., *Utilizing full-exchange capacity of zeolites by alkaline leaching: Preparation of Fe-ZSM5 and application in N2O decomposition.* Journal of Catalysis, 2006. **238**(2): p. 250-259.

55. Brandenberger, S., et al., *The determination of the activities of different iron species in Fe-ZSM-5 for SCR of NO by NH3.* Applied Catalysis B: Environmental, 2010. **95**(3–4): p. 348-357.

56. Wang, J., et al., *Improvement of low-temperature hydrothermal stability of Cu/SAPO-34 catalysts by Cu2+ species.* Journal of Catalysis, 2015. **322**(0): p. 84-90.

57. Wang, D., et al., *NH3-SCR over Cu/SAPO-34 – Zeolite acidity and Cu structure changes as a function of Cu loading.* Catalysis Today, 2014. **231**(0): p. 64-74.

58. Rahkamaa-Tolonen, K., et al., *The effect of NO2 on the activity of fresh and aged zeolite catalysts in the NH3-SCR reaction.* Catalysis Today, 2005. **100**(3–4): p. 217-222.

59. Koebel, M., G. Madia, and M. Elsener, *Selective catalytic reduction of NO and NO2 at low temperatures.* Catalysis Today, 2002. **73**(3-4): p. 239-247.

60. Long, R.Q. and R.T. Yang, *Reaction mechanism of selective catalytic reduction of NO with NH3 over Fe-ZSM-5 catalyst.* Journal of Catalysis, 2002. **207**(2): p. 224-231.

61. Delahay, G., et al., *Selective catalytic reduction of NO by NH3 on CU-faujasite catalysts: An experimental and quantum chemical approach.* ChemPhysChem, 2002. **3**(8): p. 686-692.

62. Petitto, C. and G. Delahay, *Selective catalytic reduction of NOx by NH3 on Cu-SAPO-34 catalysts: Influence of silicium content on the activity of calcined and hydrotreated samples.* Chemical Engineering Journal, 2015. **264**: p. 404-410.

63. Schwidder, M., et al., *Selective reduction of NO with Fe-ZSM-5 catalysts of low Fe content: I. Relations between active site structure and catalytic performance.* Journal of Catalysis, 2005. **231**(2): p. 314-330.

64. Park, J.-H., et al., *Hydrothermal stability of CuZSM5 catalyst in reducing NO by NH3 for the urea selective catalytic reduction process.* Journal of Catalysis, 2006. **240**(1): p. 47-57.

65. Wijayanti, K., et al., *Impact of sulfur oxide on NH3-SCR over Cu-SAPO-34.* Applied Catalysis B: Environmental, 2015. **166–167**(0): p. 568-579.

66. Mihai, O., et al., *The effect of Cu-loading on the reactions involved in ammonia SCR over Cu zeolites* J. of Catalysis, 2014. **311**: p. 170.

67. Yu, T., et al., *The influence of CO_2 and H_2O on selective catalytic reduction of NO by NH_3 over Cu/SAPO-34 catalyst.* Chemical Engineering Journal, 2015. **264**(0): p. 845-855.

68. Olsson, L., et al., *A multi-site kinetic model for NH3-SCR over Cu/SSZ-13.* Appl. Catal. B: Environmental., 2015. **174-175**: p. 212.

69. Xuan, X., et al., *Selective catalytic reduction of NO by ammonia with fly ash catalyst ☆.* Fuel, 2003. **82**(5): p. 575-579.

70. ALS Scandinavia AB, A., 977 75 Luleå. Email: info.LU@alsglobal.com, *ICP-SFMS analysis for ash*, in *Chalmers Tekniska Högskola, Program: MG2*. 2015-06-01 by App1.LU: Ordernumber: L1514212.
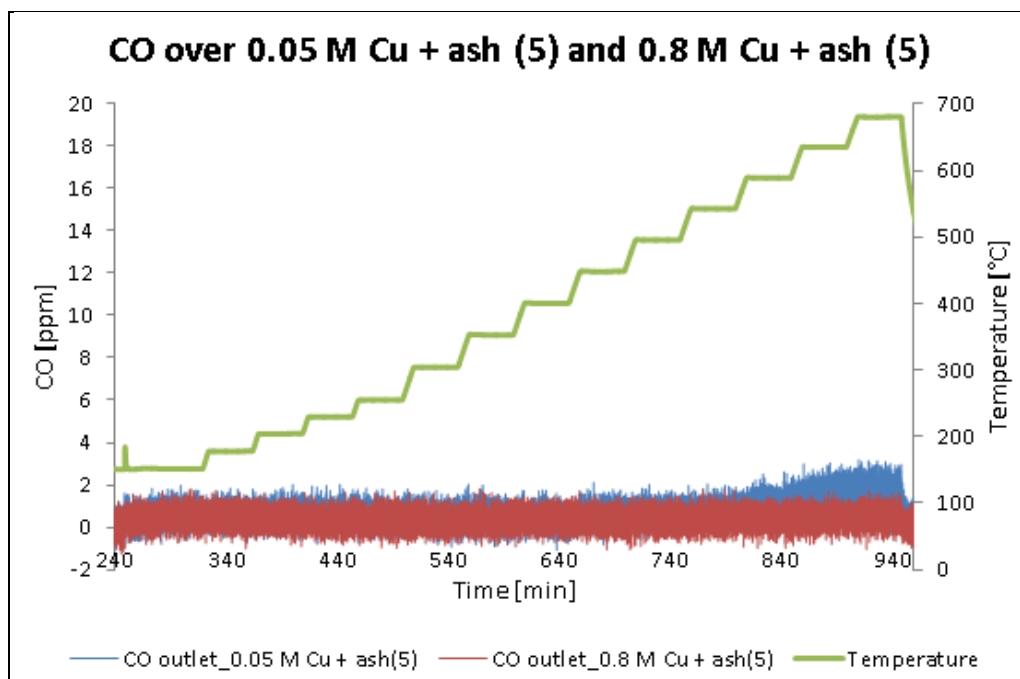
8. APPENDIX

Figure A1: CO concentration comparison between 0.05 M Cu/SAPO-34 with 5 g/L ash and 0.8 M Cu/SAPO-34 with 5 g/L ash.
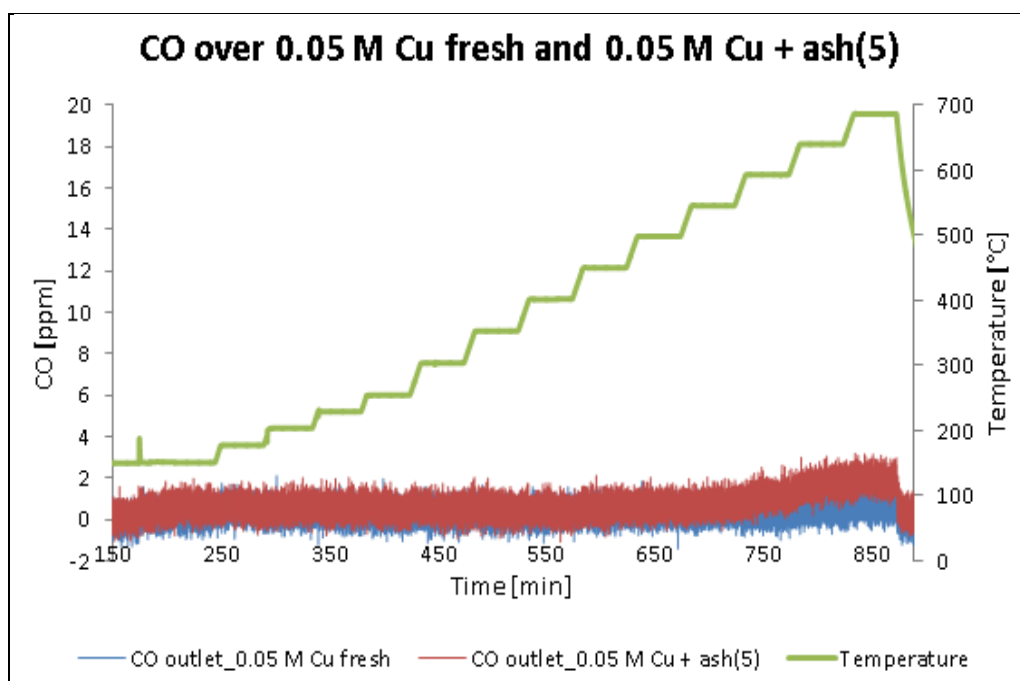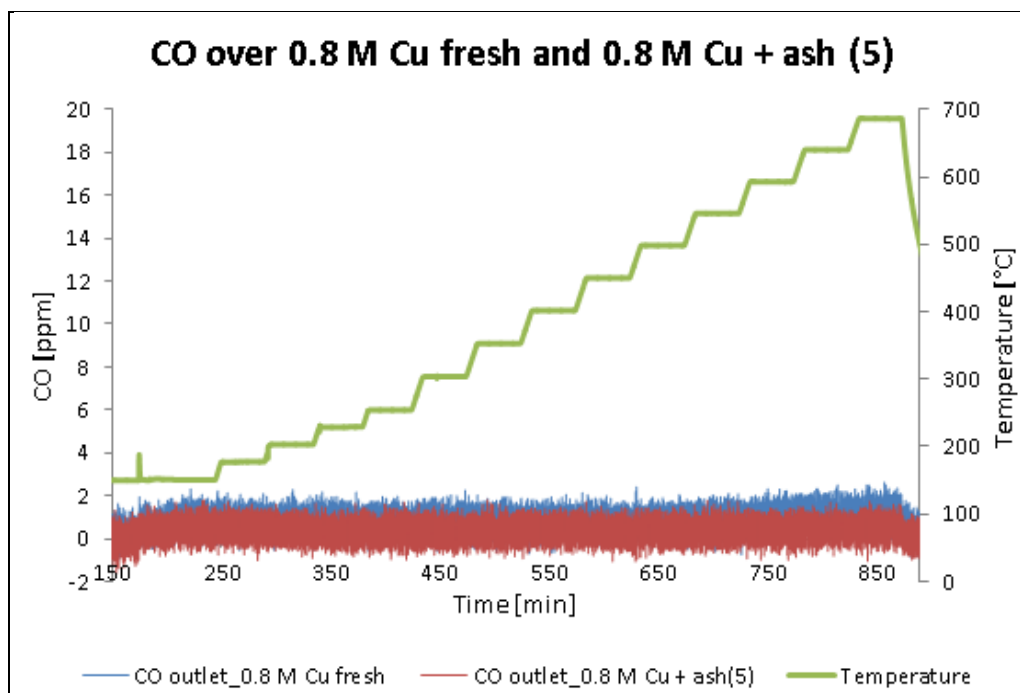

Figure A2: CO concentration comparison between fresh 0.05 M Cu/SAPO-34 and 0.05 M Cu/SAPO-34 with 5 g/L ash.

Figure A3: CO concentration comparison between fresh 0.8 M Cu/SAPO-34 and 0.8 M Cu/SAPO-34 with 5 g/L ash.